# A Fourth Order Numerical Method for the Primitive Equations Formulated in Mean Vorticity

Jian-Guo Liu[1] and Cheng Wang[2,*]

[1] *Institute for Physical Science and Technology & Department of Mathematics, University of Maryland, College Park, MD 20742-4015, USA.*
[2] *Department of Mathematics, the University of Tennessee, Knoxville, TN 37996-1300, USA.*

Received 6 October 2007; Accepted (in revised version) 6 December 2007

Available online 27 February 2008

**Abstract.** A fourth-order finite difference method is proposed and studied for the primitive equations (PEs) of large-scale atmospheric and oceanic flow based on mean vorticity formulation. Since the vertical average of the horizontal velocity field is divergence-free, we can introduce mean vorticity and mean stream function which are connected by a 2-D Poisson equation. As a result, the PEs can be reformulated such that the prognostic equation for the horizontal velocity is replaced by evolutionary equations for the mean vorticity field and the vertical derivative of the horizontal velocity. The mean vorticity equation is approximated by a compact difference scheme due to the difficulty of the mean vorticity boundary condition, while fourth-order long-stencil approximations are utilized to deal with transport type equations for computational convenience. The numerical values for the total velocity field (both horizontal and vertical) are statically determined by a discrete realization of a differential equation at each fixed horizontal point. The method is highly efficient and is capable of producing highly resolved solutions at a reasonable computational cost. The full fourth-order accuracy is checked by an example of the reformulated PEs with force terms. Additionally, numerical results of a large-scale oceanic circulation are presented.

**AMS subject classifications**: 35Q35, 65M06, 86A10

**Key words**: The primitive equations, mean vorticity, compact scheme, long-stencil approximation, one-sided extrapolation, large scale oceanic circulation.

## 1 Introduction

The primitive equations (PEs) stand for fundamental governing equations for large-scale atmospheric and oceanic flow. This system is derived from the 3-D incompressible Navier-Stokes equations (NSEs) under Boussinesq assumption that density variation is neglected

*Corresponding author. *Email addresses:* jliu@math.umd.edu (J.-C. Liu), wang@math.utk.edu (C. Wang)

 

except in the buoyancy term, combined with hydrostatic approximation for the vertical momentum equation. See a detailed derivation in J. Pedlosky [24], R. Cushman [10], J. L. Lions, R. Temam and S. Wang [18–22], etc.

In the PE system, the pressure gradient, the hydrostatic balance, are coupled together with the incompressibility of the three-dimensional velocity field. In addition, there is no momentum equation for the vertical velocity since it is replaced by the hydrostatic balance. Consequently, the vertical velocity is determined by the horizontal velocity field via an integration formula of its divergence. As a result, the degree of nonlinearity of the primitive equations is even higher than that of the usual 3-D NSEs, due to lack of regularity for the vertical velocity. This nonlinearity is one of the main difficulties of the 3-D PEs, in both the PDE level and numerical analysis.

There have been numerous papers on the PDE analysis for the PEs (for example, see [2, 3, 6, 14, 16–19]). In those papers the system is proven to be well-posed. Regarding the numerical issues, some schemes based on velocity-pressure formulation were introduced and analyzed in recent articles. In [27], J. Shen and S. Wang discuss a numerical method based on a spectral Stokes solver. In [26] by R. Samelson, R. Temam, C. Wang and S. Wang, a numerical scheme in terms of the surface pressure Poisson equation formulation is proposed, and the convergence analysis of the scheme using a 3-D MAC (marker and cell) grid is established. Some relevant numerical work can also be found in [11, 30, 31], etc.

It is well-known that for 2-D NSEs, the introduction of the vorticity-stream function formulation is highly beneficial numerically and leads to the following four distinct features: (1) the vorticity and stream function are related by a kinematic Poisson equation, (2) the pressure variable is eliminated, (3) the dynamical equation is replaced by the vorticity transport equation, and (4) the velocity field is recovered by the kinematic relationship and the incompressibility is automatically enforced. We refer to [12, 13, 34] for an extensive discussion of computational methods based on local vorticity boundary conditions. In these approaches, the Neumann boundary condition for the stream function (which comes from the no-slip boundary condition for the velocity) is converted into a local vorticity boundary formula, using the kinematic relationship between the stream function and vorticity. Such an approach can be very efficiently implemented by explicit temporal discretization.

On the other hand, the development of a corresponding vorticity formulation for 3-D geophysical flow has not been as well studied. In the context of the 3-D PEs, since the leading behavior is two-dimensional by an asymptotic description of atmosphere and ocean, the above methodology can be applied in a similar, yet more tricky way. In particular, the above-mentioned four distinct features are still reflected in our vorticity formulation and numerical method as follows.

First, the averaged horizontal velocity field in vertical direction is divergence-free, namely (2.6) and (2.7) below, due to the incompressibility of the flow and the vanishing vertical velocity at the top and bottom. This allows the concept of a mean vorticity and mean stream function to be introduced so that the kinematic relationship between the

two takes the form of a 2-D Poisson equation.

Second, by taking the vertical derivative to the original momentum equation and applying the hydrostatic balance, the pressure gradient is converted into a density gradient, resulting in an evolution equation for $v_z=(\xi,\zeta)$.

Third, the entire PE system can be reformulated in terms of evolution equations for the mean vorticity, density and $v_z=(\xi,\zeta)$.

Finally, the total velocity in horizontal direction is then determined in a kinematic way by its vertical derivative and its average from the top and bottom. The vertical velocity is also recovered in a kinematic way from solving a two-point boundary value problem at each fixed horizontal point.

The above equations form an equivalent formulation of the PEs, namely the mean vorticity formulation. This formulation was reported in [33] and the derivation of the reformulation is reviewed in Section 2.

A fourth-order scheme is a widely accepted way to improve the accuracy within the limited resolution, due to the enormous scale of the three-dimensional setting. In Section 3, we introduce a numerical method with fourth-order accuracy, based on the PEs formulated in mean vorticity. The prognostic variables, including the mean vorticity field, the profile $v_z$ and the density field, are dynamically updated. A mixed approach of compact and long stencil fourth-order difference method are utilized to deal with different variables. Regarding the scalar mean vorticity, some ideas of 2-D incompressible flow calculation can be adapted. An essentially compact scheme for 2-D NSEs was proposed in [12] and its stability and convergence were analyzed in detail in [34]. This compact approach is applied in this paper to the evolution equation for mean vorticity, with a slight modification in the nonlinear convection term. The mean vorticity field on the lateral boundary is determined by the mean stream function field through a high-order local formula, such as Briley's formula. The reason for taking compact difference is to avoid "ghost" computational grid points for mean vorticity, since the boundary layer becomes highly singular at a large Reynolds number. Yet, such a compact approach becomes computationally very expensive and highly infeasible for 3-D transport-type equations for density and $v_z$. These variables are much smoother than the mean vorticity field near the boundary. That provides the possibility of a fourth-order solver with long-stencil approximations to spatial derivatives, avoiding the computational cost of solving a 3-D Poisson-like equation involving auxiliary transport variable. Moreover, the "ghost" point values for the variables are required to implement long stencil schemes. These values are recovered by one-sided extrapolation near the boundary, using information from the original PDE to reduce the number of interior points needed in the one-sided formula for better stability property.

In turn, the total velocity field, both horizontal and vertical, are recovered by the combination of the mean velocity field and $v_z$, using FFT-based solvers. The first- and second-order vertical derivatives are approximated by long-stencil and compact differences, respectively. A detailed description of the recovery solver is provided in Section 4.

The Reynolds number for atmosphere and ocean is usually very large, hence explicit treatment for the diffusion term should be used. To avoid the cell Reynolds number constraint caused by the convection term, some multi-stage explicit temporal discretization, such as the classical fourth-order Runge-Kutta method, is suggested. In conjunction with the fourth-order spatial discretization, the resulting procedure is simple to implement and highly efficient. The main computation effort at each time step (stage) is reduced to: two 2-D Poisson-type solvers in the mean vorticity equation, explicit long stencil finite difference updating in the evolution equations for $v_z$ and density, along with fourth-order recovery for the velocity field with a careful usage of FFT solvers. The time stepping procedure is given in Section 5.

In Section 6, an accuracy check is carried out for the numerical method applied to the reformulated PEs with force terms, demonstrating fourth-order accuracy of the method.

As further evidence of the accuracy and efficiency of the method we present in Section 7 a numerical simulation of a thermocline model in oceanography, using a $256^2\times 128$ resolution. The initial density profile is composed of two constant densities (with a scaled ratio $0.97:1.03$), separated by a two-dimensional interface function. As time goes on, the thermocline profile keeps moving westward, due to the effect of Coriolis force. In addition, a wind stress is imposed at the ocean surface. Some interesting phenomenon of its interaction with the interior structure of thermocline can also be observed.

## 2 Review of the mean vorticity formulation of the primitive equations

The dimensionless form of the PEs is given by the following system under proper scaling:

$$\begin{cases} \boldsymbol{v}_t+(\boldsymbol{v}\cdot\nabla)\boldsymbol{v}+w\partial_z\boldsymbol{v}+\dfrac{1}{Ro}\Big(fk\times\boldsymbol{v}+\nabla p\Big)=\Big(\dfrac{1}{Re_1}\triangle+\dfrac{1}{Re_2}\partial_z^2\Big)\boldsymbol{v}, \\ \partial_z p=-\rho, \\ \nabla\cdot\boldsymbol{v}+\partial_z w=0, \\ \rho_t+(\boldsymbol{v}\cdot\nabla)\rho+w\partial_z\rho=\Big(\dfrac{1}{Rt_1}\triangle+\dfrac{1}{Rt_2}\partial_z^2\Big)\rho, \end{cases} \tag{2.1}$$

with the initial data

$$\boldsymbol{v}(x,y,0)=\boldsymbol{v}_0(x,y),\quad \rho(x,y,0)=\rho_0(x,y). \tag{2.2}$$

See, e.g., Pedlosky [24], Cushman [10], Lions et al. [18,19] for a detailed derivation. Some relevant issues related to geophysical flow are also extensively discussed in [7–10, 23, 30, 31], etc.

In (2.1), $\boldsymbol{u}=(\boldsymbol{v},w)=(u,v,w)$ is the 3-D velocity field, $\boldsymbol{v}=(u,v)$ the horizontal velocity, $\rho$ the density field, $p$ the pressure. The Rossby number $Ro$ measures the ratio of the velocity of the sea-water to the surface velocity of the earth in its rotation. The term $fk\times\boldsymbol{v}$ corresponds to the Coriolis force, with a $\beta-$plane approximation $f=f_0+\beta y$. To avoid

confusion, we note that the operators $\nabla$, $\nabla^{\perp}$, $\nabla\cdot$, $\triangle$ stand for the gradient, perpendicular gradient, divergence and Laplacian in horizontal $(x,y)$ plane, respectively.

For simplicity of presentation below we denote $\nu_1=1/Re_1$, $\nu_2=1/Re_2$, $\kappa_1=1/Rt_1$, and $\kappa_2=1/Rt_2$.

The PEs are derived from the Boussinesq approximation (i.e., the assumption that density variation is neglected except in the buoyancy term) with asymptotic scaling. One of its distinguishing features is the replacement of the momentum equation for the vertical velocity $w$ by the hydrostatic balance $\partial p/\partial z=-\rho$. More precisely, the momentum equation for $w$ can be written as the following with proper scaling:

$$w_t+(\boldsymbol{v}\cdot\nabla)w+w\partial_z w+\frac{1}{\delta^2}\Big(\partial_z p+\rho\Big)=\Big(\nu_1\triangle+\nu_2\partial_z^2\Big)w, \tag{2.3}$$

where the term $\delta^{-2}(\partial_z p+\rho)$ corresponds to gravity stratification of geophysical flow, with the aspect ratio $\delta=\mathcal{O}(H/L)$ ($H$ and $L$ represent the vertical and horizontal scalings, respectively). Under the assumption that $\delta$ being small, i.e., $H\ll L$, the first-order expansion of (2.3) gives the hydrostatic balance as in the PE system (2.1).

The computational domain is taken as $\mathcal{M}=\mathcal{M}_0\times[-H_0,0]$, where $\mathcal{M}_0$ is the horizontal surface occupied by the ocean. On the lateral boundary section $\partial\mathcal{M}_0\times[-H_0,0]$, the no-penetration, no-slip boundary condition is imposed for the horizontal velocity $\boldsymbol{v}$ and the no-flux boundary condition is imposed for the density field

$$\boldsymbol{v}=0,\quad\text{and}\quad\frac{\partial\rho}{\partial\boldsymbol{n}}=0,\quad\text{on }\partial\mathcal{M}_0\times[-H_0,0]. \tag{2.4}$$

The boundary condition at top surface $z=0$ and bottom surface $z=-H_0$ is taken as the following

$$\begin{aligned}&\nu_2\partial_z\boldsymbol{v}=\tau_0,\quad w=0\quad\text{and}\quad\kappa_2\partial_z\rho=\rho_f\quad\text{at } z=0,\\&\nu_2\partial_z\boldsymbol{v}=0,\quad w=0\quad\text{and}\quad\kappa_2\partial_z\rho=0\quad\text{at } z=-H_0,\end{aligned} \tag{2.5}$$

which was widely used in earlier literatures. The detailed description, derivation and analysis of the PEs in the above formulation were established by Lions et al. in [18, 19], Cao and Titi [6], etc. In this paper, the numerical method is based on the above boundary conditions. Other boundary conditions can be similarly adapted and will be discussed in the future. The term $\tau_0$ represents the wind stress force, $\rho_f$ the heat flux, at the surface of the ocean. The no-flux boundary condition for horizontal velocity field $\boldsymbol{v}_z=0$ at $z=-H_0$ is a boundary layer approximation, which states that the potential vorticity $\omega_3=-\partial_y u+\partial_x v$ has vanishing flux (normal derivative) at the bottom of the ocean. That is a reasonable assumption since there is usually no dramatic boundary layer behavior at the bottom area due to the slow motion of ocean in that region.

Some relevant works regarding the numerical simulation of the geophysical flow can be found in [11, 25–27, 30, 31], etc. This article focuses on the issue of the numerical approximation to the solution of the primitive equations (2.1), (2.2), (2.4) and (2.5) in fourth-order accuracy, using fourth-order finite differences on a regular numerical grid.

### 2.1 Introduction of mean vorticity, mean stream function and mean velocity

It should be noted that the pressure $p$ in the PEs is a Lagrange multiplier in the horizontal plane and determined by the density field in vertical direction. We aim to develop a new formulation to cancel the pressure variable. The starting point is that

$$\int_{-H_0}^{0}(\nabla\cdot\boldsymbol{v})(x,y,\cdot)dz=0,\quad \forall(x,y)\in\mathcal{M}_0, \tag{2.6}$$

or, equivalently,

$$(\nabla\cdot\overline{\boldsymbol{v}})(x,y)=0,\quad \forall(x,y)\in\mathcal{M}_0. \tag{2.7}$$

which comes from the incompressibility of $\boldsymbol{u}=(\boldsymbol{v},w)$ and the boundary condition for $w$ at $z=0,-H_0$. The divergence-free property of the mean velocity field $\overline{\boldsymbol{v}}=(\overline{u},\overline{v})$ in $(x,y)$ plane indicates an introduction of the mean stream function $\overline{\psi}$, a 2-D field, such that

$$\overline{\boldsymbol{v}}=\nabla^{\perp}\overline{\psi}=(-\partial_y\overline{\psi},\partial_x\overline{\psi}). \tag{2.8}$$

Subsequently, we defined the mean vorticity as

$$\overline{\omega}=\nabla\times\overline{\boldsymbol{v}}=-\partial_y\overline{u}+\partial_x\overline{v}. \tag{2.9}$$

It should be noted that $\overline{\omega}$ defined above is the same as the average of the potential vorticity in vertical direction $\omega_3=\nabla\times\boldsymbol{v}=-u_y+v_x$. Furthermore, the kinematic relationship between the mean stream function and the mean vorticity can be written in terms of the following 2-D Poisson equation

$$\triangle\overline{\psi}=\overline{\omega}. \tag{2.10}$$

### 2.2 The reformulation of the PEs

The PE system can be reformulated as follows.
*Mean vorticity equation*

$$\begin{cases}\overline{\omega}_t+(\nabla^{\perp}\cdot\nabla\cdot)\left(\overline{\boldsymbol{v}\otimes\boldsymbol{v}}\right)+\dfrac{\beta}{Ro}\overline{v}=\nu_1\triangle\overline{\omega}+\dfrac{1}{H_0}\nabla^{\perp}\cdot\tau_0,\\ \triangle\overline{\psi}=\overline{\omega},\\ \overline{\psi}=0,\quad \dfrac{\partial\overline{\psi}}{\partial\boldsymbol{n}}=0,\quad \text{on }\partial\mathcal{M}_0,\\ \overline{\boldsymbol{v}}=\nabla^{\perp}\overline{\psi}=(-\partial_y\overline{\psi},\partial_x\overline{\psi}),\end{cases} \tag{2.11}$$

*Evolutionary equation for* $\boldsymbol{v}_z=(\xi,\zeta)$

$$\begin{cases}\boldsymbol{v}_{zt}+\begin{pmatrix}u\xi_x+v\xi_y+w\xi_z-v_y\xi+u_y\zeta\\ u\zeta_x+v\zeta_y+w\zeta_z-u_x\zeta+v_x\xi\end{pmatrix}+\dfrac{f}{Ro}k\times\boldsymbol{v}_z-\dfrac{1}{Ro}\nabla\rho=\left(\nu_1\triangle+\nu_2\partial_z^2\right)\boldsymbol{v}_z,\\ \boldsymbol{v}_z|_{z=0}=\dfrac{1}{\nu_2}\tau_0,\quad \boldsymbol{v}_z|_{z=-H_0}=0,\\ \boldsymbol{v}_z=0,\quad \text{on}\quad \partial\mathcal{M}_0\times[-H_0,0],\end{cases} \tag{2.12}$$

*Recovery of the horizontal velocity*

$$\begin{cases} \partial_z u=\xi, \qquad \partial_z v=\zeta, \\ \dfrac{1}{H_0}\displaystyle\int_{-H_0}^{0} \boldsymbol{v}dz=\overline{\boldsymbol{v}}. \end{cases} \tag{2.13}$$

*Recovery of the vertical velocity*

$$\begin{cases} \partial_z^2 w=-\nabla\cdot\boldsymbol{v}_z=-\xi_x-\zeta_y, \\ w=0, \qquad \text{at} \quad z=0,-H_0. \end{cases} \tag{2.14}$$

*Density transport equation*

$$\begin{cases} \rho_t+(\boldsymbol{v}\cdot\nabla)\rho+w\partial_z\rho=\Big(\kappa_1\triangle+\kappa_2\partial_z^2\Big)\rho, \\ \partial_z\rho\,|_{z=0}=\dfrac{\rho_f}{\kappa_2}, \quad \partial_z\rho\,|_{z=-H_0}=0, \quad \dfrac{\partial\rho}{\partial\boldsymbol{n}}\,|_{\partial\mathcal{M}_0\times[-H_0,0]}=0. \end{cases} \tag{2.15}$$

The detailed derivation can be found in [33]. Note that the momentum equations in (2.1) can be rewritten as

$$\begin{cases} u_t+(uu)_x+(uv)_y+(uw)_z-\dfrac{f}{Ro}v+\dfrac{1}{Ro}\partial_x p=\Big(\nu_1\triangle+\nu_2\partial_z^2\Big)u, \\ v_t+(uv)_x+(vv)_y+(vw)_z+\dfrac{f}{Ro}u+\dfrac{1}{Ro}\partial_y p=\Big(\nu_1\triangle+\nu_2\partial_z^2\Big)v, \end{cases} \tag{2.16}$$

which comes from the incompressibility of $\boldsymbol{u}=(u,v,w)$. Taking the average of (2.16) over $[-H_0,0]$ gives

$$\partial_t\overline{\boldsymbol{v}}+\nabla\cdot\Big(\overline{\boldsymbol{v}\otimes\boldsymbol{v}}\Big)+\frac{f}{Ro}k\times\overline{\boldsymbol{v}}+\frac{1}{Ro}\nabla\overline{p}=\nu_1\triangle\overline{\boldsymbol{v}}+\frac{1}{H_0}\tau_0, \tag{2.17}$$

where the average of the velocity tensor product turns out to be

$$\overline{\boldsymbol{v}\otimes\boldsymbol{v}}=\begin{pmatrix} \overline{uu} & \overline{uv} \\ \overline{uv} & \overline{vv} \end{pmatrix}. \tag{2.18}$$

The terms $\overline{(uw)_z}$, $\overline{(vw)_z}$ disappear because of the boundary condition for $w$ at $z=0,-H_0$. The force term in (2.17) comes from the integration of $\partial_z^2\boldsymbol{v}$ and the boundary condition for $\boldsymbol{v}$ at the top and bottom sections. Consequently, taking the curl operator $\nabla^\perp\cdot$ to (2.17) gives the dynamic equation for the mean vorticity in (2.11), which is a scalar equation. For simplicity of presentation, the nonlinear convection term can be written in the form of matrix product,

$$\begin{aligned} (\nabla^\perp\cdot\nabla\cdot)\Big(\overline{\boldsymbol{v}\otimes\boldsymbol{v}}\Big)&=\begin{pmatrix} -\partial_{xy} & -\partial_y^2 \\ \partial_x^2 & \partial_{xy} \end{pmatrix}:\begin{pmatrix} \overline{uu} & \overline{uv} \\ \overline{uv} & \overline{vv} \end{pmatrix} \\ &=\partial_{xy}\Big(-\overline{uu}+\overline{vv}\Big)+\Big(\partial_x^2-\partial_y^2\Big)\overline{uv}. \end{aligned} \tag{2.19}$$

The kinematic relation in (2.11) comes from (2.8), (2.10). The boundary condition for $\overline{\psi}$ in (2.11) is a direct result of the homogeneous boundary condition $\overline{v}|_{\partial\mathcal{M}_0}=0$ (because of the boundary condition for $v$ on $\partial\mathcal{M}_0\times[-H_0,0]$ in (2.4)). Note that there are two boundary conditions for $\overline{\psi}$, including both Dirichlet and Neumann. The numerical difficulty associated with this issue will be discussed later.

It should be noted that (2.11) is not a closed system for the mean profiles $\overline{\omega}$, $\overline{\psi}$, $\overline{v}$, since in the nonlinear convection term $\overline{v\otimes v}$ is not equal to $\overline{v}\otimes\overline{v}$. To update the total velocity field $v$, we need additional information of $v_z$.

Taking the vertical derivative of the momentum equation (2.16) leads to the following system for $v_z=(\xi,\zeta)$, with Dirichlet boundary condition on all boundary sections

$$\begin{cases} \partial_t v_z+\mathcal{N}LF+\dfrac{f}{Ro}k\times v_z-\dfrac{1}{Ro}\nabla\rho=\Big(\nu_1\triangle+\nu_2\partial_z^2\Big)v_z, \\ v_z|_{z=0}=\dfrac{1}{\nu_1}\tau_0, \quad v_z|_{z=-H_0}=0, \\ v_z=0, \quad \text{on} \quad \partial\mathcal{M}_0\times[-H_0,0]. \end{cases} \tag{2.20}$$

The nonlinear term $\mathcal{N}LF=(f_1,f_2)$ is evaluated as the following by using the incompressibility condition $u_x+v_y+w_z=0$:

$$\begin{aligned} f_1&=\partial_z\Big(uu_x+vu_y+wu_z\Big)=u\xi_x+v\xi_y+w\xi_z-v_y\xi+u_y\zeta, \\ f_2&=\partial_z\Big(uv_x+vv_y+wv_z\Big)=u\zeta_x+v\zeta_y+w\zeta_z-u_x\zeta+v_x\xi. \end{aligned} \tag{2.21}$$

With the combination of $\overline{v}$ and $v_z$ at hand, which can be obtained by solving (2.11), (2.12), respectively, the horizontal velocity field is determined by (2.13), a system of ordinary differential equations.

In addition, by taking the vertical derivative of the continuity equation $\nabla\cdot v+\partial_z w=0$, we get (2.14), a system of second-order ODEs for the vertical velocity with the vanishing Dirichlet boundary condition. Both (2.13) and (2.14) can be solved at any fixed horizontal point $(x,y)$.

The density transport equation (2.15) is the same as that in (2.1)-(2.5). This finishes the derivation of the reformulation (2.11)-(2.15).

**Remark 2.1.** In [6], Cao and Titi analyzed the system of the PEs with a boundary condition for the velocity $u$ on the lateral boundary section imposed as: normal component of velocity being 0, and the normal derivative of the horizontal derivative $v$ being 0. In this case, the mean vorticity field vanishes identically on the lateral boundary, which can be easily implemented in our numerical scheme. This is also one of the main reasons why there is a global strong solution for the corresponding system. This boundary condition is also a realistic one as the viscosity boundary layer has little effect to large-scale oceanic flow model. In this paper, we consider the 3-D PEs with a no-penetration, no-slip boundary condition on the later boundary.

# 3 Fourth-order spatial discretization for the PEs

For simplicity, we consider the computational domain as $\mathcal{M}_0=[0,1]^2$, $H_0=1$. The regular uniform grid with mesh size $\triangle x=\triangle y=\triangle z=h=\frac{1}{N}$ is used in the calculation. Let $\tilde{D}_x$, $\tilde{D}_y$, $\tilde{D}_z$ represent the standard second-order centered-difference approximations to $\partial_x$, $\partial_y$, $\partial_z$, $D_x^2$, $D_y^2$, $D_z^2$ the second-order centered-difference approximations to $\partial_x^2$, $\partial_y^2$, $\partial_z^2$, and $\triangle_h=D_x^2+D_y^2$ the standard five-point Laplacian.

## 3.1 Compact scheme for the mean vorticity equation

In this section we describe the compact difference scheme for the mean vorticity evolution equation. The starting point is the fourth-order approximation to the 2-D Laplacian operator $\triangle$,

$$\triangle=\frac{\triangle_h+\frac{h^2}{6}D_x^2D_y^2}{1+\frac{h^2}{12}\triangle_h}+\mathcal{O}(h^4); \tag{3.1}$$

see [32] for a relevant derivation. The following equation can be obtained by multiplying the denominator difference operator $1+h^2\triangle_h/12$ to (2.11):

$$\begin{aligned}&(1+\frac{h^2}{12}\triangle_h)\partial_t\overline{\omega}+(1+\frac{h^2}{12}\triangle_h)\Big(\partial_x\partial_y(\overline{v}\overline{v}-\overline{u}\overline{u})+(\partial_x^2-\partial_y^2)\overline{u}\overline{v}+\frac{\beta}{Ro}\overline{v}\Big)\\&=\nu_1\Big(\triangle_h+\frac{h^2}{6}D_x^2D_y^2\Big)\overline{\omega}+f_{\overline{\omega}},\end{aligned} \tag{3.2}$$

where the force

$$f_{\overline{\omega}}=\frac{1}{H_0}\Big(1+\frac{h^2}{12}\triangle_h\Big)(\nabla^{\perp}\cdot\tau_0)$$

is a known term.

The nonlinear convection terms in (3.2) can be evaluated by the following Taylor expansion:

$$(1+\frac{h^2}{12}\triangle_h)\partial_x\partial_y=\Big(1-\frac{\triangle x^2}{12}D_x^2-\frac{\triangle y^2}{12}D_y^2\Big)\tilde{D}_x\tilde{D}_y+\mathcal{O}(h^4), \tag{3.3}$$

$$(1+\frac{h^2}{12}\triangle_h)(\partial_x^2-\partial_y^2)=D_x^2-D_y^2+\frac{1}{12}(\triangle y^2-\triangle x^2)D_x^2D_y^2+\mathcal{O}(h^4). \tag{3.4}$$

Therefore, by the introduction of an intermediate variable $\overline{\omega}^*$,

$$\overline{\omega}^*=(1+\frac{h^2}{12}\triangle_h)\overline{\omega}, \tag{3.5}$$

which is defined at interior grid points $(x_i,y_j)$, $1\le i,j\le N-1$, the mean vorticity evolution equation can be approximated by

$$\begin{aligned}&\partial_t\overline{\omega}^*+\Big(1-\frac{\triangle x^2}{12}D_x^2-\frac{\triangle y^2}{12}D_y^2\Big)\tilde{D}_x\tilde{D}_y(\overline{\overline{v}\overline{v}}^S-\overline{\overline{u}\overline{u}}^S)\\&+\Big(D_x^2-D_y^2+\frac{1}{12}(\triangle y^2-\triangle x^2)D_x^2D_y^2\Big)\overline{\overline{u}\overline{v}}^S+\frac{\beta}{Ro}(1+\frac{h^2}{12}\triangle_h)\overline{v}\\&=\nu_1\Big(\triangle_h+\frac{h^2}{6}D_x^2D_y^2\Big)\overline{\omega}+f_{\overline{\omega}},\end{aligned}\tag{3.6}$$

where the Simpson rule is used to define the fourth-order vertical average of any variable $f$ in vertical direction

$$\overline{\overline{f}}^S_{i,j}=\frac{1}{H_0}\frac{\triangle z}{3}\Big(f_{i,j,0}+f_{i,j,N}+4\sum_{k=1}^{\frac{N_z}{2}}f_{i,j,2k-1}+2\sum_{k=1}^{\frac{N_z}{2}-1}f_{i,j,2k}\Big).\tag{3.7}$$

Note that all terms in (3.6) are compact except for the first convection terms, which requires the "ghost" computational point values for $\overline{\overline{v}\overline{v}}$, $\overline{\overline{u}\overline{u}}$. This can be accomplished by a high-order extrapolation.

The substitution of (3.1) into the kinematic relation between the mean stream function and mean vorticity results in

$$\Big(\triangle_h+\frac{h^2}{6}D_x^2D_y^2\Big)\overline{\psi}=\overline{\omega}^*,\tag{3.8}$$

which is a fourth-order approximation. Thus the mean stream function can be solved by the above compact difference system, with the Dirichlet boundary condition $\overline{\psi}|_{\partial\mathcal{M}_0}=0$. The mean velocity field $\overline{v}=\nabla^\top\overline{\psi}=(-\partial_y\overline{\psi},\partial_x\overline{\psi})$ can be obtained by a fourth-order long-stencil approximation to $\partial_x$, $\partial_y$,

$$\overline{u}=-\tilde{D}_y(1-\frac{h^2}{6}D_y^2)\overline{\psi},\quad \overline{v}=\tilde{D}_x(1-\frac{h^2}{6}D_x^2)\overline{\psi}.\tag{3.9}$$

After the intermediate mean vorticity field $\overline{\omega}^*$ is updated by the scheme (3.6), the original mean vorticity can be determined by the Poisson-like equation (3.5). The solver for the system (3.5) requires the boundary value for $\overline{\omega}$, which is discussed below.

**Boundary condition for mean vorticity.** Physically speaking, the vorticity boundary condition enforces the no-slip boundary condition. The vorticity at the boundary is computed by some local formula, which is derived from the combination of the kinematic relation $\omega=\triangle\psi$ with the no-slip boundary condition $\partial\psi/\partial\boldsymbol{n}=0$. One-sided approximation and high-order Taylor expansion for stream function around the boundary was used in the derivation of these local formulas.

A similar idea can be applied to the primitive equations formulated in mean vorticity. A local boundary formula for mean vorticity is obtained in the same way. Briley's

formula was initially proposed in [4] and its application into EC4 scheme was analyzed in [12, 34]. On the boundary section $\Gamma_x$, where $j=0$, Briley's formula reads

$$\overline{\omega}_{i,0}=\frac{1}{18h^2}(108\overline{\psi}_{i,1}-27\overline{\psi}_{i,2}+4\overline{\psi}_{i,3}). \tag{3.10}$$

The corresponding "ghost" point values for stream function are given by

$$\overline{\psi}_{i,-1}=6\overline{\psi}_{i,1}-2\overline{\psi}_{i,2}+\frac{1}{3}\overline{\psi}_{i,3}-4h\left(\frac{\partial\overline{\psi}}{\partial y}\right)_{i,0}+\mathcal{O}(h^5), \tag{3.11}$$

$$\overline{\psi}_{i,-2}=40\overline{\psi}_{i,1}-15\overline{\psi}_{i,2}+\frac{8}{3}\overline{\psi}_{i,3}-12h\left(\frac{\partial\overline{\psi}}{\partial y}\right)_{i,0}+\mathcal{O}(h^5). \tag{3.12}$$

It was shown in [34] that the Briley's formula, a one-sided vorticity boundary condition, preserves stability and is consistent with the compact difference method applied at interior points.

### 3.2 Long stencil scheme for evolution equation of $v_z$

The compact scheme used for the mean vorticity equation turns out to be computationally very expensive for the evolutionary equations for $v_z=(\xi,\zeta)$ and density transport equation, since a linear system solver is needed to recover the auxiliary variable. The well-defined Dirichlet boundary condition for $(\xi,\zeta)$ and the Neumann boundary condition for the density, provide the possibility of fourth-order solvers without using an auxiliary variable. The spatial derivatives in the equation are treated by long-stencil fourth-order approximations, requiring the numerical values at "ghost" points. These values are recovered by one-sided extrapolation near the boundary using information from the original PDE.

The standard fourth-order centered long-stencil approximation to the derivatives $\partial_x$, $\partial_y$, $\partial_z$ is given by

$$\begin{aligned}
\partial_x&=\tilde{D}_x(1-\frac{h^2}{6}D_x^2)+\mathcal{O}(h^4),\\
\partial_y&=\tilde{D}_y(1-\frac{h^2}{6}D_y^2)+\mathcal{O}(h^4),\\
\partial_z&=\tilde{D}_z(1-\frac{h^2}{6}D_z^2)+\mathcal{O}(h^4).
\end{aligned} \tag{3.13}$$

Similarly, $\partial_x^2$, $\partial_y^2$, $\partial_z^2$ can be approximated in a similar fashion,

$$\begin{aligned}
\partial_x^2&=D_x^2(1-\frac{h^2}{12}D_x^2)+\mathcal{O}(h^4),\\
\partial_y^2&=D_y^2(1-\frac{h^2}{12}D_y^2)+\mathcal{O}(h^4),\\
\partial_z^2&=D_z^2(1-\frac{h^2}{12}D_z^2)+\mathcal{O}(h^4).
\end{aligned} \tag{3.14}$$

The substitution of the long-stencil formulas into (2.12) gives the spatial discretization of the evolution equations for $(\xi,\zeta)$:

$$\begin{aligned}
&\partial_t\xi+u\tilde{D}_x(1-\frac{h^2}{6}D_x^2)\xi+v\tilde{D}_y(1-\frac{h^2}{6}D_y^2)\xi+w\tilde{D}_z(1-\frac{h^2}{6}D_z^2)\xi\\
&\quad-\xi\tilde{D}_y(1-\frac{h^2}{6}D_y^2)v+\zeta\tilde{D}_y(1-\frac{h^2}{6}D_y^2)u-\frac{f}{Ro}\zeta-\frac{1}{Ro}\tilde{D}_x(1-\frac{h^2}{6}D_x^2)\rho\\
&=\Big(\nu_1(D_x^2-\frac{h^2}{12}D_x^4+D_y^2-\frac{h^2}{12}D_y^4)+\nu_2(D_z^2-\frac{h^2}{12}D_z^4)\Big)\xi, \qquad (3.15)\\
&\partial_t\zeta+u\tilde{D}_x(1-\frac{h^2}{6}D_x^2)\zeta+v\tilde{D}_y(1-\frac{h^2}{6}D_y^2)\zeta+w\tilde{D}_z(1-\frac{h^2}{6}D_z^2)\zeta\\
&\quad-\zeta\tilde{D}_x(1-\frac{h^2}{6}D_x^2)u+\xi\tilde{D}_x(1-\frac{h^2}{6}D_x^2)v+\frac{f}{Ro}\xi-\frac{1}{Ro}\tilde{D}_y(1-\frac{h^2}{6}D_y^2)\rho\\
&=\Big(\nu_1(D_x^2-\frac{h^2}{12}D_x^4+D_y^2-\frac{h^2}{12}D_y^4)+\nu_2(D_z^2-\frac{h^2}{12}D_z^4)\Big)\zeta. \qquad (3.16)
\end{aligned}$$

**Ghost point values for $(\xi,\zeta)$.** Determination of $v_z=(\xi,\zeta)$ at "ghost" points is needed at the six boundary sections to implement the finite difference scheme (3.15), (3.16).

On the bottom surface $z=-H_0$, $\xi_{i,j,0}$ and $\zeta_{i,j,0}$ are exactly given to be 0, due to the Dirichlet boundary condition. The difference equations (3.15), (3.16) are then updated at interior points $(x_i,y_j,z_k)$, $1\le k\le N-1$, requiring the prescription of the "ghost" point values of $\xi_{i,j,-1}$, $\zeta_{i,j,-1}$ due to the stencil used in the discretization. A local Taylor expansion for $v_z=(\xi,\zeta)$ in fifth-order near the boundary section $z=-H_0$ reads

$$\begin{aligned}
\xi_{i,j,-1}&=\frac{20}{11}\xi_{i,j,0}-\frac{6}{11}\xi_{i,j,1}-\frac{4}{11}\xi_{i,j,2}+\frac{1}{11}\xi_{i,j,3}+\frac{12}{11}\triangle z^2\partial_z^2\xi_{i,j,0}+\mathcal{O}(h^5),\\
\zeta_{i,j,-1}&=\frac{20}{11}\zeta_{i,j,0}-\frac{6}{11}\zeta_{i,j,1}-\frac{4}{11}\zeta_{i,j,2}+\frac{1}{11}\zeta_{i,j,3}+\frac{12}{11}\triangle z^2\partial_z^2\zeta_{i,j,0}+\mathcal{O}(h^5).
\end{aligned} \qquad (3.17)$$

The implementation of (3.17) requires an accurate evaluation of $\partial_z^2\xi$ and $\partial_z^2\zeta$ for $k=0$. Such terms are prescribed by considering the evolution equations for $v_z=(\xi,\zeta)$ at the boundary $\Gamma_z$, $z=-H_0$:

$$\begin{aligned}
\partial_t\xi\,|_{\Gamma_z}-\frac{1}{Ro}(\partial_x\rho)\,|_{\Gamma_z}&=\nu_1(\partial_x^2+\partial_y^2)\xi\,|_{\Gamma_z}+\nu_2\partial_z^2\xi\,|_{\Gamma_z},\\
\partial_t\zeta\,|_{\Gamma_z}-\frac{1}{Ro}(\partial_y\rho)\,|_{\Gamma_z}&=\nu_1(\partial_x^2+\partial_y^2)\zeta\,|_{\Gamma_z}+\nu_2\partial_z^2\zeta\,|_{\Gamma_z}.
\end{aligned} \qquad (3.18)$$

The nonlinear convection terms vanish because of the boundary condition $(\xi,\zeta)\,|_{\Gamma_z}=0$ and the vertical velocity $w$ being identically 0 on the bottom. Furthermore, we have

$$\begin{aligned}
\partial_z^2\xi\,|_{z=-H_0}&=-\frac{1}{\nu_2\cdot Ro}\partial_x\rho\,|_{z=-H_0},\\
\partial_z^2\zeta\,|_{z=-H_0}&=-\frac{1}{\nu_2\cdot Ro}\partial_y\rho\,|_{z=-H_0}.
\end{aligned} \qquad (3.19)$$

The terms $\rho_x$, $\rho_y$ on $z=-H_0$ can be calculated by the standard fourth-order long-stencil formula, i.e.,

$$\begin{aligned}\partial_z^2\xi\,|_{z=-H_0}&=-\frac{1}{\nu_2\cdot Ro}\tilde{D}_x(1-\frac{h^2}{6}D_x^2)\rho_{i,j,0}+\mathcal{O}(h^4),\\ \partial_z^2\zeta\,|_{z=-H_0}&=-\frac{1}{\nu_2\cdot Ro}\tilde{D}_y(1-\frac{h^2}{6}D_y^2)\rho_{i,j,0}+\mathcal{O}(h^4).\end{aligned}\tag{3.20}$$

The substitution of (3.20) into (3.17) leads to

$$\begin{aligned}\xi_{i,j,-1}=&\frac{20}{11}\xi_{i,j,0}-\frac{6}{11}\xi_{i,j,1}-\frac{4}{11}\xi_{i,j,2}+\frac{1}{11}\xi_{i,j,3}\\&-\frac{12}{11\nu_2 Ro}\triangle z^2\tilde{D}_x(1-\frac{h^2}{6}D_x^2)\rho_{i,j,0}+\mathcal{O}(h^5),\\ \zeta_{i,j,-1}=&\frac{20}{11}\zeta_{i,j,0}-\frac{6}{11}\zeta_{i,j,1}-\frac{4}{11}\zeta_{i,j,2}+\frac{1}{11}\zeta_{i,j,3}\\&-\frac{12}{11\nu_2 Ro}\triangle z^2\tilde{D}_y(1-\frac{h^2}{6}D_y^2)\rho_{i,j,0}+\mathcal{O}(h^5).\end{aligned}\tag{3.21}$$

An analogous derivation can be carried out on the top boundary section $z=0$ and lateral boundary sections $x=0,1$, $y=0,1$. Note that there are some force terms appearing in the extrapolation formula for $(\xi,\zeta)$ at the top if a non-vanishing wind stress $\tau_0$ is prescribed. The detail is left for interested readers. It can be demonstrated that the above formulas lead to full fourth-order accuracy. The proof will appear in a forthcoming article.

**Remark 3.1.** Instead of the fifth-order one-sided approximation near the boundary $z=-H_0$ in (3.17), a fourth-order Taylor expansion near the boundary can also be used, which results in only one interior point in the formula

$$\begin{aligned}\xi_{i,j,-1}&=2\xi_{i,j,0}-\xi_{i,j,1}+\triangle z^2\partial_z^2\xi_{i,j,0}+\mathcal{O}(h^4),\\ \zeta_{i,j,-1}&=2\zeta_{i,j,0}-\zeta_{i,j,1}+\triangle z^2\partial_z^2\zeta_{i,j,0}+\mathcal{O}(h^4).\end{aligned}\tag{3.22}$$

The derivation of $\partial_z^2\xi_{i,j,0}$, $\partial_z^2\zeta_{i,j,0}$ on $z=-H_0$ as shown in (4.18)-(4.20) is also valid. The combination of (3.22) and (3.20) leads to

$$\begin{aligned}\xi_{i,j,-1}&=2\xi_{i,j,0}-\xi_{i,j,1}-\frac{1}{\nu_2 Ro}\triangle z^2\tilde{D}_x(1-\frac{h^2}{6}D_x^2)\rho_{i,j,0}+\mathcal{O}(h^4),\\ \zeta_{i,j,-1}&=2\zeta_{i,j,0}-\zeta_{i,j,1}-\frac{1}{\nu_2 Ro}\triangle z^2\tilde{D}_y(1-\frac{h^2}{6}D_y^2)\rho_{i,j,0}+\mathcal{O}(h^4).\end{aligned}\tag{3.23}$$

which is an $\mathcal{O}(h^4)$ formula analogous to (3.21). The numerical evidence shows that both (3.21) and (3.23) provide stability and full accuracy. The fourth-order formula (3.23) brings computational convenience since it requires only one interior point. However, for technical considerations in the stability and convergence analysis of the overall scheme, which will appear in a forthcoming article, the fifth-order approximation (3.21) is preferred.

### 3.3 Long-stencil scheme for the density transport equation

Similarly, the transport equation for the density as given in (2.15) can be solved in fourth-order accuracy without introducing an auxiliary variable due to the well-defined Neumann boundary condition. Long-stencil fourth-order difference operators are used to approximate the spatial derivatives corresponding to convection and diffusion terms, in which the numerical values at "ghost" points are required near the boundary. One-sided extrapolation near the boundary using information from the original transport equation in the PDE level is applied to recover these values.

The standard fourth-order centered long-stencil differences (3.13), (3.14) are chosen to approximate the derivatives $\partial_x$, $\partial_y$, $\partial_z$, $\partial_x^2$, $\partial_y^2$ and $\partial_z^2$. Consequently, the spatial discretization of the density transport equation can be written as

$$\begin{aligned}&\partial_t\rho+u\tilde{D}_x(1-\frac{h^2}{6}D_x^2)\rho+v\tilde{D}_y(1-\frac{h^2}{6}D_y^2)\rho+w\tilde{D}_z(1-\frac{h^2}{6}D_z^2)\rho\\&=\Big(\kappa_1(D_x^2-\frac{h^2}{12}D_x^4+D_y^2-\frac{h^2}{12}D_y^4)+\kappa_2(D_z^2-\frac{h^2}{12}D_z^4)\Big)\rho.\end{aligned}\tag{3.24}$$

**Ghost point values for $\rho$.** Since the Neumann boundary condition is imposed in (2.15), the density profile on the boundary is not known explicitly, only its normal derivative. As a result, (3.24) is applied at every computational point $(x_i,y_j,z_k)$, $0\le i,j,k\le N$, while the determination of two "ghost" point values, e.g., $\rho_{i,j,-1}$ and $\rho_{i,j,-2}$ around the bottom boundary section $z=-H_0$, is required.

We begin by deriving one-sided approximations. Local Taylor expansion near the bottom boundary $z=-H_0$ gives

$$\begin{aligned}\rho_{i,j,-1}&=\rho_{i,j,1}-2\triangle z\partial_z\rho_{i,j,0}-\frac{\triangle z^3}{3}\partial_z^3\rho_{i,j,0}+\mathcal{O}(h^5),\\\rho_{i,j,-2}&=\rho_{i,j,2}-4\triangle z\partial_z\rho_{i,j,0}-\frac{8\triangle z^3}{3}\partial_z^3\rho_{i,j,0}+\mathcal{O}(h^5),\end{aligned}\tag{3.25}$$

in which the term $\partial_z\rho_{i,j,0}$ is known to vanish because of the no-flux boundary condition for the density. The remaining work is focused on the determination of $\partial_z^3\rho$ at $k=0$, for which we use information from the PDE and its derivatives. In more detail, applying the normal derivative $\partial_z$ to the density transport equation along $z=-H_0$ leads to

$$\rho_{zt}+u_z\rho_x+u\rho_{zx}+v_z\rho_y+v\rho_{zy}+w_z\rho_z+w\rho_{zz}=\kappa_1(\rho_{zxx}+\rho_{zyy})+\kappa_2\partial_z^3\rho,\quad\text{at } z=-H_0.\tag{3.26}$$

Using the no-flux boundary condition for $\rho$ and the vanishing boundary condition for $w$ at $z=-H_0$, we have

$$\partial_z^3\rho=\frac{1}{\kappa_2}\Big(u_z\rho_x+v_z\rho_y\Big),\qquad\text{at}\quad z=-H_0,\tag{3.27}$$

whose combination with the vanishing boundary condition for $(u_z,v_z)=(\xi,\zeta)$ at $z=-H_0$ results in

$$\partial_z^3\rho=0, \qquad \text{at} \quad z=-H_0. \tag{3.28}$$

Inserting (3.28) into (3.25) gives

$$\rho_{i,j,-1}=\rho_{i,j,1}+\mathcal{O}(h^5), \qquad \rho_{i,j,-2}=\rho_{i,j,2}+\mathcal{O}(h^5), \tag{3.29}$$

in which the no-flux boundary condition for $\rho$ is recalled.

Analogous formulas for one-sided extrapolation of $\rho_{i,j,N+1}$, $\rho_{i,j,N+2}$ around the top boundary $z=0$ can be derived in a similar way. The evaluation for the normal derivative of the original PDE as shown in (3.26), (3.27) is still valid. Furthermore, the wind stress boundary condition for $v_z=(\xi,\zeta)$ at the top $z=0$, combined with the fourth-order long-stencil approximation to $\rho_x$, $\rho_y$ gives

$$\partial_z^3\rho=\frac{1}{\kappa_2\cdot\nu_2}\Big(\tau_{0,1}\tilde{D}_x(1-\frac{h^2}{6}D_x^2)\rho+\tau_{0,2}\tilde{D}_y(1-\frac{h^2}{6}D_y^2)\rho\Big)+\mathcal{O}(h^4), \qquad \text{at} \quad z=0. \tag{3.30}$$

Therefore, we arrive at an extrapolation formula for the density field around the top boundary,

$$\begin{aligned}
\rho_{i,j,N+1}&=\rho_{i,j,N-1}+\frac{\triangle z^3}{3\kappa_2\cdot\nu_2}\Big(\tau_{0,1}\tilde{D}_x(1-\frac{h^2}{6}D_x^2)\rho_{i,j,N}+\tau_{0,2}\tilde{D}_y(1-\frac{h^2}{6}D_y^2)\rho_{i,j,N}\Big)+\mathcal{O}(h^5),\\
\rho_{i,j,N+2}&=\rho_{i,j,N-2}+\frac{8\triangle z^3}{3\kappa_2\cdot\nu_2}\Big(\tau_{0,1}\tilde{D}_x(1-\frac{h^2}{6}D_x^2)\rho_{i,j,N}+\tau_{0,2}\tilde{D}_y(1-\frac{h^2}{6}D_y^2)\rho_{i,j,N}\Big)+\mathcal{O}(h^5).
\end{aligned} \tag{3.31}$$

The corresponding derivation for the one-sided extrapolation for $\rho$ around the four lateral boundary sections can be performed in a similar fashion. We skip it for the sake of conciseness. The detail is left for interested readers.

# 4 Fourth-order recovery of the velocity field

The remaining work is focused on the determination of the horizontal and vertical velocity field. It is based on differential equations (1.9c,d), which plays the role of a bridge between the total velocity field and the mean profile and $v_z=(\xi,\zeta)$.

## 4.1 Recovery for the horizontal velocity field

The total horizontal velocity field is determined by the combination of $v_z=(\xi,\zeta)$ and the mean velocity field $\overline{v}$. At the interior grid points $(i,j,k)$ with $1\le k\le N-1$, where the numerical values of $\xi$, $\zeta$ are given, we apply the fourth-order long-stencil difference operator in vertical direction to approximate (2.13)

$$\tilde{D}_z(1-\frac{h^2}{6}D_z^2)u=\xi, \qquad \tilde{D}_z(1-\frac{h^2}{6}D_z^2)v=\zeta, \qquad \text{at} \quad (i,j,k), \quad 1\le k\le N-1, \tag{4.1}$$

in which four numerical points of $(u,v)$ are involved for each $k$. Meanwhile, the mean velocity field $\overline{v}=(\overline{u},\overline{v})$, which is determined by the fourth-order difference of the mean stream function field as shown in (3.9), is assigned to be the vertically discrete average of the horizontal velocity field $v=(u,v)$ using Simpson's rule, i.e.,

$$\begin{aligned}\overline{\overline{u}}^S_{i,j}&=\frac{1}{H_0}\frac{\triangle z}{3}\Big(u_{i,j,0}+u_{i,j,N}+4\sum_{k=1}^{\frac{N_z}{2}}u_{i,j,2k-1}+2\sum_{k=1}^{\frac{N_z}{2}-1}u_{i,j,2k}\Big)=\overline{u}_{i,j},\\ \overline{\overline{v}}^S_{i,j}&=\frac{1}{H_0}\frac{\triangle z}{3}\Big(v_{i,j,0}+v_{i,j,N}+4\sum_{k=1}^{\frac{N_z}{2}}v_{i,j,2k-1}+2\sum_{k=1}^{\frac{N_z}{2}-1}v_{i,j,2k}\Big)=\overline{v}_{i,j}.\end{aligned}\tag{4.2}$$

Note that $(\xi,\zeta)$ vanishes at the bottom $k=0$ and its top boundary profile at $k=N$ is given by $\frac{1}{\nu_2}\tau_0$. For simplicity we set $\tau_0=0$, and the extension to the case of non-homogeneous wind stress profile is straightforward. In addition, the "ghost" numerical value for $(u,v)$ at $k=-1,N+1$ are required to solve (4.1). To achieve fourth-order accuracy, we perform local Taylor expansion for $v=(u,v)$ in fifth-order near the boundary section $z=-H_0$:

$$\begin{aligned}u_{i,j,-1}&=u_{i,j,1}-2\triangle z\partial_z u_{i,j,0}-\frac{\triangle z^3}{3}\partial_z^3 u_{i,j,0}+\mathcal{O}(h^5),\\ v_{i,j,-1}&=v_{i,j,1}-2\triangle z\partial_z v_{i,j,0}-\frac{\triangle z^3}{3}\partial_z^3 v_{i,j,0}+\mathcal{O}(h^5).\end{aligned}\tag{4.3}$$

The term $\partial_z u$, $\partial_z v$ disappears at $z=-H_0$ because of the boundary condition imposed for $(\xi,\zeta)$. The accurate evaluation of $\partial_z^3\xi$, $\partial_z^3\zeta$ follows that in (3.18)-(3.20) in Section 3, by using the original PDE along the bottom boundary. An alternate form of (3.20) reads

$$\begin{aligned}(\partial_z^3 u)\,|_{z=-H_0}&=-\frac{1}{\nu_2}\tilde{D}_x(1-\frac{h^2}{6}D_x^2)\rho_{i,j,0}+\mathcal{O}(h^4),\\ (\partial_z^3 v)\,|_{z=-H_0}&=-\frac{1}{\nu_2}\tilde{D}_y(1-\frac{h^2}{6}D_y^2)\rho_{i,j,0}+\mathcal{O}(h^4),\end{aligned}\tag{4.4}$$

because of the definition for $(\xi,\zeta)$. The combination of (4.4) and (4.3) gives

$$\begin{aligned}u_{i,j,-1}&=u_{i,j,1}+\frac{\triangle z^3}{3\nu_2}\tilde{D}_x(1-\frac{h^2}{6}D_x^2)\rho_{i,j,0}+\mathcal{O}(h^5),\\ v_{i,j,-1}&=v_{i,j,1}+\frac{\triangle z^3}{3\nu_2}\tilde{D}_y(1-\frac{h^2}{6}D_y^2)\rho_{i,j,0}+\mathcal{O}(h^5).\end{aligned}\tag{4.5}$$

Similar derivation for the "ghost" point value extrapolation around the top boundary $z=0$ for $(u,v)$ can be performed:

$$\begin{aligned}u_{i,j,N+1}&=u_{i,j,N-1}+\frac{\triangle z^3}{3\nu_2}\tilde{D}_x(1-\frac{h^2}{6}D_x^2)\rho_{i,j,N}+\mathcal{O}(h^5),\\ v_{i,j,N+1}&=v_{i,j,N-1}+\frac{\triangle z^3}{3\nu_2}\tilde{D}_y(1-\frac{h^2}{6}D_y^2)\rho_{i,j,N}+\mathcal{O}(h^5).\end{aligned}\tag{4.6}$$

Note that the correction term in (4.5), (4.6) can be moved to the right side of (4.1). In other words, we could denote $\xi_f$, $\zeta_f$ as the profile of $(\xi,\zeta)$ with the high-order correction terms added, thus the system (4.1), (4.5), (4.6) can be rewritten as

$$\tilde{D}_z(1-\frac{h^2}{6}D_z^2)u=\xi_f,\quad \tilde{D}_z(1-\frac{h^2}{6}D_z^2)v=\zeta_f,\quad \text{at}\quad (i,j,k),\quad 1\le k\le N-1, \tag{4.7}$$

$$u_{i,j,-1}=u_{i,j,1},\quad v_{i,j,-1}=v_{i,j,1},\quad u_{i,j,N+1}=u_{i,j,N-1},\quad v_{i,j,N+1}=v_{i,j,N-1}. \tag{4.8}$$

The coupled system of (4.2), (4.7), (4.8) forms the linear system we are going to deal with.

Since the basis function $\cos(\pi z_k)$ is a complete set of eigenfunction for the fourth-order centered difference $\tilde{D}_z(1-\frac{h^2}{6}D_z^2)$, the system (4.2), (4.7), (4.8) can be solved by using FFT. The "ghost" point boundary condition for $\boldsymbol{v}=(u,v)$ in (4.8) makes it feasible to perform Cosine transformation in vertical direction for each fixed $(i,j)$, i.e.,

$$\begin{aligned} u_{i,j,k}&=\frac{1}{\sqrt{2N_z}}\left[\hat{u}_{i,j,0}+\sum_{l=1}^{N_z-1}(2\hat{u}_{i,j,l})\cos\Big(\frac{lk\pi}{N_z}\Big)+(-1)^k\hat{u}_{i,j,N}\right],\\ v_{i,j,k}&=\frac{1}{\sqrt{2N_z}}\left[\hat{v}_{i,j,0}+\sum_{l=1}^{N_z-1}(2\hat{v}_{i,j,l})\cos\Big(\frac{lk\pi}{N_z}\Big)+(-1)^k\hat{v}_{i,j,N}\right]. \end{aligned} \tag{4.9}$$

The determination of the Fourier modes $\hat{\boldsymbol{v}}_{i,j,l}$, $l=0,1,\cdots,N_z$, is based on the difference equation (4.7) and the constraint (4.2) for the mean velocity field. First we observe that

$$\begin{aligned} &\tilde{D}_z(1-\frac{h^2}{6}D_z^2)\hat{\boldsymbol{v}}_{i,j,0}=0,\\ &\tilde{D}_z(1-\frac{h^2}{6}D_z^2)\cos\Big(lk\pi h\Big)=f_l^{'}\cdot\sin\Big(lk\pi h\Big),\\ &\tilde{D}_z(1-\frac{h^2}{6}D_z^2)\Big((-1)^k\Big)=0, \end{aligned} \tag{4.10}$$

with the coefficients $f_l^{'}$

$$f_l^{'}=-\frac{\sin\Big(l\pi h\Big)}{\triangle z}\left[1-\frac{2}{3}\sin^2\Big(\frac{l\pi h}{2}\Big)\right]. \tag{4.11}$$

Going back to (4.9), we arrive at

$$\begin{aligned} \Big(\tilde{D}_z(1-\frac{h^2}{6}D_z^2)u\Big)_{i,j,k}&=\frac{2}{\sqrt{2N_z}}\sum_{l=1}^{N_z-1}f_l^{'}\hat{u}_{i,j,l}\sin\Big(\frac{lk\pi}{N_z}\Big),\\ \Big(\tilde{D}_z(1-\frac{h^2}{6}D_z^2)u\Big)_{i,j,k}&=\frac{2}{\sqrt{2N_z}}\sum_{l=1}^{N_z-1}f_l^{'}\hat{v}_{i,j,l}\sin\Big(\frac{lk\pi}{N_z}\Big). \end{aligned} \tag{4.12}$$

Meanwhile, the sine transformation in Fourier space for $\xi_f$, $\zeta_f$ can be made due to the homogeneous Dirichlet boundary condition at $k=0,N$, i.e.,

$$(\xi_f)_{i,j,k}=\sum_{l=1}^{N_z-1}\frac{2\hat{\xi}_{f\,i,j,l}}{\sqrt{2N_z}}\sin\Big(\frac{lk\pi}{N_z}\Big),\quad \zeta_{i,j,k}=\sum_{l=1}^{N_z-1}\frac{2\hat{\zeta}_{f\,i,j,l}}{\sqrt{2N_z}}\sin\Big(\frac{lk\pi}{N_z}\Big). \tag{4.13}$$

Comparing (4.13) with (4.12), we see that the equation (4.7) is exactly satisfied if

$$\hat{u}_{i,j,l}=\frac{\hat{\xi}_{f\,i,j,l}}{f_l'},\quad \hat{v}_{i,j,l}=\frac{\hat{\zeta}_{f\,i,j,l}}{f_l'},\qquad \text{for}\quad 1\le l\le N_z-1, \tag{4.14}$$

with $f_l'$ given by (4.11).

To obtain the 0-th Fourier mode coefficient for $\boldsymbol{v}$ at each fixed grid point $(i,j)$, we see that the application of Simpson's rule to the horizontal velocity profile $\boldsymbol{v}=(u,v)$ represented in the Fourier expansion (4.9) gives

$$\frac{1}{H_0}N_z\triangle z\frac{1}{\sqrt{2N_z}}\hat{u}_{i,j,0}=\overline{u}_{i,j}+\mathcal{O}(h^4),\qquad \frac{1}{H_0}N_z\triangle z\frac{1}{\sqrt{2N_z}}\hat{v}_{i,j,0}=\overline{v}_{i,j}+\mathcal{O}(h^4), \tag{4.15}$$

since the basis functions $\cos(kl\pi h)$ have vanishing discrete average in the vertical direction using Simpson's rule, for $l=1,2,\cdots,N_z$, provided that $N_z$ is even. As a result, we choose

$$\hat{u}_{i,j,0}=\sqrt{2N_z}\overline{u}_{i,j},\qquad \hat{v}_{i,j,0}=\sqrt{2N_z}\overline{v}_{i,j}. \tag{4.16}$$

In addition, since the Fourier mode coefficients $\hat{\boldsymbol{v}}_{i,j,l}$ decay exponentially as $l$ approaches $N_z$ under suitable regularity assumption for the velocity field, we can set the coefficient $\hat{\boldsymbol{v}}_{i,j,N}$ to be 0. In other words,

$$\hat{u}_{i,j,N}=\hat{v}_{i,j,N}=0. \tag{4.17}$$

Then the procedure to solve the system (4.2), (4.7), (4.8) can be outlined as follows: (1) move the correction terms in (4.5), (4.6) to the right side of (4.1) to obtain the profile $(\xi_f,\zeta_f)$; (2) sine transform the profile $(\xi_f,\zeta_f)$ as in (4.13); (3) obtain the Fourier coefficients (in the cosine transformation) for $\boldsymbol{v}$ by (4.14), (4.16) and (4.17); (4) cosine transform $\boldsymbol{v}$ at each fixed grid point $(i,j)$ as in (4.9).

### 4.2 Recovery for the vertical velocity field

The vertical velocity $w$ can be solved by a compact fourth-order scheme of the second-order O.D.E (2.14). The second-order derivative $\partial_z^2$ can be approximated by

$$\partial_z^2=\frac{D_z^2}{1+\frac{\triangle z^2}{12}D_z^2}+\mathcal{O}(h^4). \tag{4.18}$$

Then we have the following fourth-order scheme

$$\begin{cases} D_z^2 w = -\Big(1+\dfrac{\triangle z^2}{12}D_z^2\Big)\Big(\tilde{D}_x(1-\dfrac{h^2}{6}D_x^2)\xi - \tilde{D}_y(1-\dfrac{h^2}{6}D_y^2)\zeta\Big), \ \text{for } 1\le k\le N_z-1, \\ w_{i,j,0}=w_{i,j,N}=0. \end{cases} \tag{4.19}$$

At each fixed horizontal grid point $(i,j)$, there are $N-1$ equations and $N-1$ unknowns: $w_{i,j,k}$ at interior grid points $1\le k\le N_z-1$. Moreover, the complete set of the eigenvalues corresponding to the operator $D_z^2$ (under the homogeneous Dirichlet boundary condition for $w$) is given by

$$\lambda_l = -\frac{4}{\triangle z^2}\sin^2\Big(\frac{l\pi}{2N_z}\Big), \qquad \text{for} \quad 1\le l\le N_z-1, \tag{4.20}$$

which are non-zero. As a result, (4.19) is a non-singular linear system at each fixed horizontal grid point.

## 5 Temporal discretization

The classical fourth-order Runge-Kutta method, a multi-stage explicit time stepping procedure, is used as the time discretization in the mean vorticity equation, evolution equation for $v_z$ and density equation. The explicit treatment of convection and diffusion terms appearing in the dynamic equations makes the whole scheme very easy to implement. Such an explicit treatment can avoid any stability concern caused by the cell-Reynolds number constraint if the high-order Runge-Kutta method, such as the classical RK4, is applied.

At each stage in Runge-Kutta time stepping, two standard 2-D Poisson-like equations, in Steps 4 and 6 below, are required to be solved. In addition, a recovery procedure for both the horizontal and vertical velocities, in Steps 8 and 9 below, needs to be performed. These can be done by FFT-based methods. The rest is the standard finite-difference updating of the computed profiles. This shows the efficiency of the method.

For simplicity, we only present the forward Euler time-discretization. The extension to the Runge-Kutta method is straightforward.

**Time-stepping**: Given $(\overline{\omega}^*)^n$, $v_z^n$ and $\rho^n$ at time $t^n$, we compute all the profiles at the time step $t^{n+1}$ via the following steps.

*Step 1.* Update $\Big\{(\overline{\omega}^*)_{i,j}^{n+1}\Big\}$, at interior points $(x_i,y_j)$ in horizontal plane, for $1\le i,j\le N-1$, by

$$\begin{aligned} &\frac{(\overline{\omega}^*)^{n+1}-(\overline{\omega}^*)^n}{\triangle t} + \Big(1-\frac{\triangle x^2}{12}D_x^2-\frac{\triangle y^2}{12}D_y^2\Big)\tilde{D}_x\tilde{D}_y\Big((\overline{\overline{vv}}^S)^n-(\overline{\overline{uu}}^S)^n\Big) \\ &\quad+\Big(D_x^2-D_y^2+\frac{1}{12}(\triangle y^2-\triangle x^2)D_x^2D_y^2\Big)(\overline{\overline{uv}}^S)^n+\frac{\beta}{Ro}(1+\frac{h^2}{12}\triangle_h)\overline{v}^n \\ &=\nu_1\Big(\triangle_h+\frac{h^2}{6}D_x^2D_y^2\Big)\overline{\omega}^n+f_{\overline{\omega}}^n, \end{aligned} \tag{5.1}$$

*Step 2.* Update $\left\{\xi_{i,j}^{n+1}\right\}$, $\left\{\zeta_{i,j}^{n+1}\right\}$ at 3-D interior points $(x_i,y_j,z_k)$, for $1\le i,j,k\le N-1$, by

$$\begin{aligned}
&\frac{\xi^{n+1}-\xi^n}{\triangle t}+u^n\tilde{D}_x(1-\frac{h^2}{6}D_x^2)\xi^n+v^n\tilde{D}_y(1-\frac{h^2}{6}D_y^2)\xi^n+w^n\tilde{D}_z(1-\frac{h^2}{6}D_z^2)\xi^n\\
&-\xi^n\tilde{D}_y(1-\frac{h^2}{6}D_y^2)v^n+\zeta^n\tilde{D}_y(1-\frac{h^2}{6}D_y^2)u^n-\frac{f}{Ro}\zeta^n-\frac{1}{Ro}\tilde{D}_x(1-\frac{h^2}{6}D_x^2)\rho^n\\
=&\Big(\nu_1(D_x^2-\frac{h^2}{12}D_x^4+D_y^2-\frac{h^2}{12}D_y^4)+\nu_2(D_z^2-\frac{h^2}{12}D_z^4)\Big)\xi^n, \qquad (5.2)\\
&\frac{\zeta^{n+1}-\zeta^n}{\triangle t}+u^n\tilde{D}_x(1-\frac{h^2}{6}D_x^2)\zeta^n+v^n\tilde{D}_y(1-\frac{h^2}{6}D_y^2)\zeta^n+w^n\tilde{D}_z(1-\frac{h^2}{6}D_z^2)\zeta^n\\
&-\zeta^n\tilde{D}_x(1-\frac{h^2}{6}D_x^2)u^n+\xi^n\tilde{D}_x(1-\frac{h^2}{6}D_x^2)v^n+\frac{f}{Ro}\xi^n-\frac{1}{Ro}\tilde{D}_y(1-\frac{h^2}{6}D_y^2)\rho^n\\
=&\Big(\nu_1(D_x^2-\frac{h^2}{12}D_x^4+D_y^2-\frac{h^2}{12}D_y^4)+\nu_2(D_z^2-\frac{h^2}{12}D_z^4)\Big)\zeta^n. \qquad (5.3)
\end{aligned}$$

The one-sided extrapolation (3.21) is applied.

*Step 3.* Update $\left\{\rho_{i,j,k}^{n+1}\right\}$, at all numerical grid points $(x_i,y_j,z_k)$, for $0\le i,j,k\le N$, by

$$\begin{aligned}
&\frac{\rho^{n+1}-\rho^n}{\triangle t}+u^n\tilde{D}_x(1-\frac{h^2}{6}D_x^2)\rho^n+v^n\tilde{D}_y(1-\frac{h^2}{6}D_y^2)\rho^n+w^n\tilde{D}_z(1-\frac{h^2}{6}D_z^2)\rho^n\\
=&\Big(\kappa_1(D_x^2-\frac{h^2}{12}D_x^4+D_y^2-\frac{h^2}{12}D_y^4)+\kappa_2(D_z^2-\frac{h^2}{12}D_z^4)\Big)\rho^n. \qquad (5.4)
\end{aligned}$$

The one-sided extrapolation (3.31) is applied.

*Step 4.* Solve for $\left\{\overline{\psi}_{i,j}^{n+1}\right\}_{1\le i,j\le N-1}$ using

$$\begin{cases}\Big(\triangle_h+\dfrac{h^2}{6}D_x^2D_y^2\Big)\overline{\psi}^{n+1}=(\overline{\omega}^*)^{n+1},\\ \overline{\psi}^{n+1}|_{\partial\mathcal{M}_0}=0,\end{cases} \qquad (5.5)$$

where only sine transformations are needed. Compute $\psi^{n+1}$ at the "ghost" points using (3.11), (3.12) (together with Briley's vorticity boundary condition (3.10)). We note that solving (5.5) only requires $(\overline{\omega}^*)^{n+1}$ at interior points $(x_i,y_j)$, $1\le i,j\le N-1$, which has been updated in Step 1.

*Step 5.* Obtain the boundary value for $\overline{\omega}^{n+1}$ by Briley's formula (3.10).

*Step 6.* Now we use the boundary values for $\overline{\omega}^{n+1}$ updated in Step 5 to solve for $\left\{\overline{\omega}_{i,j}^{n+1}\right\}_{i\ge1,j\ge1}$ using

$$\Big(1+\frac{h^2}{12}\triangle_h\Big)\overline{\omega}^{n+1}=(\overline{\omega}^*)^{n+1}. \qquad (5.6)$$

*Step 7.* Update the mean velocity field $\overline{v}_{i,j}^{n+1}$ using the centered difference of mean stream function

$$\overline{u}^{n+1}=-\tilde{D}_y(1-\frac{h^2}{6}D_y^2)\overline{\psi}^{n+1},\qquad \overline{v}^{n+1}=\tilde{D}_x(1-\frac{h^2}{6}D_x^2)\overline{\psi}^{n+1}, \tag{5.7}$$

for $i,j\geq 1$, and $\overline{v}^{n+1}=0$ on $\partial\mathcal{M}_0$.

*Step 8.* With both $\overline{v}^{n+1}$ and $v_z^{n+1}$ at hand, which are determined and updated in Steps 6 and 2, respectively, we are able to get the total horizontal velocity field at $t^{n+1}$ with the help of the procedure given in Section 4.1, namely, the solution of the following system

$$\begin{cases} \tilde{D}_z(1-\frac{h^2}{6}D_z^2)u^{n+1}=\xi_f^{n+1}, \quad \tilde{D}_z(1-\frac{h^2}{6}D_z^2)v^{n+1}=\zeta_f^{n+1}, \quad \text{for } 1\leq k\leq N-1, \\ (\overline{\overline{u}}^S)_{i,j}^{n+1}=\overline{u}_{i,j}^{n+1}, \quad (\overline{\overline{v}}^S)_{i,j}^{n+1}=\overline{v}_{i,j}^{n+1}, \\ u_{i,j,-1}^{n+1}=u_{i,j,1}^{n+1}, \quad v_{i,j,-1}^{n+1}=v_{i,j,1}^{n+1}, \quad u_{i,j,N+1}^{n+1}=u_{i,j,N-1}^{n+1}, \quad v_{i,j,N+1}^{n+1}=v_{i,j,N-1}^{n+1}, \end{cases} \tag{5.8}$$

in which the numerical average $\overline{\overline{v}}$ is given by the definition in (4.2).

*Step 9.* Recover the vertical velocity field $w^{n+1}$ by

$$\begin{cases} D_z^2 w^{n+1}=-\Big(1+\dfrac{\triangle z^2}{12}D_z^2\Big)\Big(\tilde{D}_x(1-\dfrac{h^2}{6}D_x^2)\xi^{n+1}-\tilde{D}_y(1-\dfrac{h^2}{6}D_x^2)\zeta^{n+1}\Big), \\ w_{i,j,0}^{n+1}=w_{i,j,N}^{n+1}=0. \end{cases} \tag{5.9}$$

## 6 Numerical accuracy check

In this section we perform an accuracy check for the proposed fourth-order method. The domain is $\mathcal{M}=\mathcal{M}_0\times[-H_0,0]$, with $\mathcal{M}_0=[0,1]^2$ and $H_0=1$. The exact profile for the mean stream function is chosen as

$$\overline{\psi}_e(x,y,t)=\frac{1}{2\pi^3}\sin^2(\pi x)\sin^2(\pi y)\cos t, \tag{6.1}$$

which satisfies no penetration, no slip boundary condition on the lateral boundary $\partial\mathcal{M}_0$. The corresponding exact mean velocity and mean vorticity are given by

$$\begin{aligned} \overline{u}_e(x,y,t)&=-\frac{1}{2\pi^2}\sin^2(\pi x)\sin(2\pi y)\cos t, \\ \overline{v}_e(x,y,t)&=\frac{1}{2\pi^2}\sin(2\pi x)\sin^2(\pi y)\cos t, \\ \overline{\omega}_e(x,y,t)&=\frac{1}{\pi}\Big(\sin^2(\pi x)\cos(2\pi y)+\sin^2(\pi y)\cos(2\pi x)\Big)\cos t. \end{aligned} \tag{6.2}$$

The exact profile of $\boldsymbol{v}_z=(\xi,\zeta)$ is given by

$$\begin{aligned}\xi_e(x,y,z,t)&=\frac{1}{2\pi}\sin^2(\pi x)\sin(2\pi y)\sin(\pi z)\cos t,\\ \zeta_e(x,y,z,t)&=-\frac{1}{\pi}\sin(2\pi x)\sin^2(\pi y)\sin(2\pi z)\cos t.\end{aligned}\tag{6.3}$$

Then the total horizontal velocity field $\boldsymbol{v}_e$ is determined by the combination of (6.2) and (6.3):

$$\begin{aligned}u_e(x,y,z,t)&=-\frac{1}{2\pi^2}\sin^2(\pi x)\sin(2\pi y)\Big(1+\cos(\pi z)\Big)\cos t,\\ v_e(x,y,z,t)&=\frac{1}{2\pi^2}\sin(2\pi x)\sin^2(\pi y)\Big(1+\cos(2\pi z)\Big)\cos t.\end{aligned}\tag{6.4}$$

Moreover, the vertical velocity $w_e$ is determined by $(\xi_e,\zeta_e)$ via (2.14):

$$w_e(x,y,z,t)=\frac{1}{2\pi}\sin(2\pi x)\sin(2\pi y)\Big(\frac{1}{\pi}\sin(\pi z)-\frac{1}{2\pi}\sin(2\pi z)\Big)\cos t.\tag{6.5}$$

The density field is chosen as

$$\rho_e(x,y,z,t)=\frac{1}{\pi^2}\cos(\pi x)\cos(\pi y)\cos(\pi z)\cos t,\tag{6.6}$$

which satisfies the no-flux boundary condition on all six boundary sections.

We can substitute the exact profiles (6.1)-(6.6) into the reformulated PE system (2.11)-(2.15). Note that there are force terms in the mean vorticity equation, evolutionary equation for $\boldsymbol{v}_z$ and density equations. The fourth-order method as described in Section 3, along with the fourth-order recovery for the velocity field in Section 4 and the explicit time stepping utilizing the classical RK4, is used to solve the system of the PEs with the force terms. The viscosity parameters are given by $\nu_1=\nu_2=0.005$, $\kappa_1=\kappa_2=0.005$ and the Rossby number is chosen as $Ro=1$.

Table 1 lists the absolute errors between the numerical and exact solutions for velocity and density. As shown in the table, perfect fourth-order accuracy in $L^1$, $L^2$ norms is obtained for the horizontal velocity field $(u,v)$. The corresponding order of accuracy in the $L^\infty$ norm converges to 4 as the grid is refined. Slightly less than fourth-order accuracy in both $L^1$, $L^2$ norms and the $L^\infty$ norm for the vertical velocity field $w$ are preserved. Again, the order of accuracy becomes closer and closer to 4 as the grid is refined. The lack of perfect accuracy for the vertical velocity field is due to the fact that $w$ is determined by the (discrete) long-stencil gradient of the profile $(\xi,\zeta)$. The accuracy for the density field is slightly less than fourth-order with coarse grid and converges to almost perfect fourth-order with the refined grid. It can be observed that the proposed fourth-order scheme indeed preserves almost perfect fourth-order accuracy for all the variables.

Table 1: Error and order of accuracy for velocity and density of the PEs formulated in mean vorticity at $t=1$ when the fourth-order spatial discretization combined with classical RK4 time stepping are used. We take $\triangle t=\frac{1}{4}\triangle x$.

| | $N$ | $L^1$ error | $L^1$ order | $L^2$ error | $L^2$ order | $L^\infty$ error | $L^\infty$ order |
|---|---|---|---|---|---|---|---|
| $u$ | 16 | 8.74e-06 | | 1.20e-05 | | 4.46e-05 | |
| | 32 | 5.54e-07 | 3.98 | 7.51e-07 | 3.99 | 2.83e-06 | 3.98 |
| | 64 | 3.45e-08 | 4.00 | 4.67e-08 | 4.00 | 1.78e-07 | 3.99 |
| | 128 | 2.15e-09 | 4.00 | 2.91e-09 | 4.00 | 1.11e-08 | 4.00 |
| $v$ | 16 | 9.60e-06 | | 1.35e-05 | | 4.30e-05 | |
| | 32 | 6.09e-07 | 3.98 | 8.50e-07 | 3.99 | 2.77e-06 | 3.96 |
| | 64 | 3.80e-08 | 4.00 | 5.30e-08 | 4.00 | 1.74e-07 | 3.99 |
| | 128 | 2.37e-09 | 4.00 | 3.31e-09 | 4.00 | 1.09e-08 | 4.00 |
| $w$ | 16 | 8.98e-06 | | 1.51e-05 | | 8.05e-05 | |
| | 32 | 5.89e-07 | 3.93 | 9.56e-07 | 3.98 | 5.15e-06 | 3.97 |
| | 64 | 3.73e-08 | 3.98 | 5.99e-08 | 3.99 | 3.23e-07 | 3.99 |
| | 128 | 2.34e-09 | 3.99 | 3.75e-09 | 4.00 | 2.02e-08 | 4.00 |
| $\rho$ | 16 | 1.54e-06 | | 2.06e-06 | | 6.13e-06 | |
| | 32 | 1.04e-07 | 3.89 | 1.35e-07 | 3.93 | 3.91e-07 | 3.97 |
| | 64 | 6.70e-09 | 3.96 | 8.53e-09 | 3.98 | 2.47e-08 | 3.98 |
| | 128 | 4.22e-10 | 3.99 | 5.34e-10 | 4.01 | 1.54e-09 | 4.00 |

## 7 Numerical results of oceanic circulation

Much effort has been devoted to the study of large-scale oceanic circulation during the past decades; see the relevant references [1, 5, 7, 9, 15, 24, 28, 29], etc. For mid-latitude oceanic regions, large scale motion is dominated by wind-driven (horizontal) and thermohaline (vertical) circulations, the two most important sources of climate low frequency variability.

In this section we give a numerical simulation of a simplified model which contains the basic features of the thermocline circulation in mid-latitude ocean, to illustrate its detailed structures in both the horizontal and vertical directions. Such a motion can be modeled as the evolution between two densities which are separated by an interface, along with an interaction with the wind stress at the ocean surface. In this simplified mode, the scaled computational domain is taken as $\mathcal{M}=[0,1]^2\times[-1,0]$. The initial density (temperature) (at $t=0$) is given by

$$\rho_0(x,y,z)=\begin{cases}\rho_2=0.97, & \text{if } z\geq z_0(x,y)+\frac{1}{64},\\ 1-0.004\sin\Big(32\pi(z-z_0(x,y)\Big), & \text{if } |z-z_0(x,y)|\leq\frac{1}{64},\\ \rho_2=1.03, & \text{if } z\leq z_0(x,y)-\frac{1}{64}.\end{cases} \tag{7.1}$$

The initial interface function is chosen as

$$z_0(x,y) = -h(x,y,0) = -h_1(x,y)[1-h_1(x,y)] - 0.125, \tag{7.2}$$

where $h(x,y,0)$ represents the initial height function and $h_1(x,y)$ is given by

$$h_1(x,y) = \begin{cases} \exp\Big(1-\dfrac{1}{1-16r^2}\Big), & \text{if } r^2 = (x-\dfrac{1}{2})^2+(y-\dfrac{1}{2})^2 \le \dfrac{1}{16}, \\ 0, \quad \text{otherwise.} \end{cases} \tag{7.3}$$

The initial horizontal velocity is set to be

$$\begin{aligned} u(x,y,z,t=0) &= -0.4\pi\cos(\pi y)\sin(\pi y)\big(x-p_1(x)\big)^2\Big(1+\sin(\frac{1}{2}\pi z)\Big), \\ v(x,y,z,t=0) &= 0.4\sin^2(\pi y)\big(x-p_1(x)\big)\big(1-p_2(x)\big)\Big(1+\sin(\frac{1}{2}\pi z)\Big), \end{aligned} \tag{7.4}$$

where $r=0.05$, and

$$p_1(x) = \frac{1-\exp(-x/r)}{1-\exp(-1/r)}, \quad p_2(x) = \frac{1/r\cdot\exp(-x/r)}{1-\exp(-1/r)}.$$

Note that the vertical average of $\boldsymbol{v}\,|_{t=0}$ is divergence-free:

$$\begin{aligned} \overline{u}(x,y,t=0) &= -0.4\pi(1-\frac{2}{\pi})\cos(\pi y)\sin(\pi y)\big(x-p_1(x)\big)^2, \\ \overline{v}(x,y,t=0) &= 0.4(1-\frac{2}{\pi})\sin^2(\pi y)\big(x-p_1(x)\big)\big(1-p_2(x)\big). \end{aligned} \tag{7.5}$$

Accordingly, the initial mean stream function turns out to be

$$\overline{\psi}(x,y,t=0) = 0.2(1-\frac{2}{\pi})\sin^2(\pi y)\big(x-p_1(x)\big)^2, \tag{7.6}$$

so that the kinematic relationship between $\overline{\psi}$ and $\overline{v}$ is satisfied. Applying the vertical derivative of (7.4) gives the initial data for $\partial_z \boldsymbol{v} = (\xi,\zeta)$:

$$\begin{aligned} \xi(x,y,z,t=0) &= -0.2\pi^2\cos(\pi y)\sin(\pi y)\big(x-p_1(x)\big)^2\cos(\frac{1}{2}\pi z), \\ \zeta(x,y,z,t=0) &= 0.2\pi\sin^2(\pi y)\big(x-p_1(x)\big)\big(1-p_2(x)\big)\cos(\frac{1}{2}\pi z). \end{aligned} \tag{7.7}$$

In particular, there is no velocity flux at the bottom $z=-1$ and the wind stress at the ocean surface $z=0$ is given by

$$\begin{aligned} &\partial_z u = -0.2\pi^2\cos(\pi y)\sin(\pi y)\big(x-p_1(x)\big)^2, \quad \text{at } z=0, \\ &\partial_z v = 0.2\pi\sin^2(\pi y)\big(x-p_1(x)\big)\big(1-p_2(x)\big), \quad \text{at } z=0, \\ &\partial_z \boldsymbol{v} = 0, \quad \text{at } z=-1. \end{aligned} \tag{7.8}$$

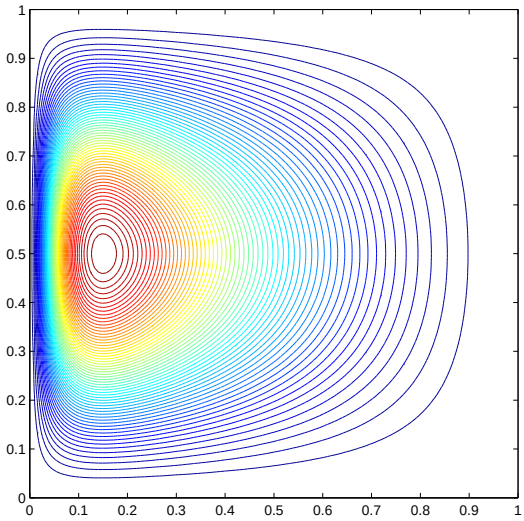


Figure 1: Contour plot of the mean stream function at $t=0$.

Note that the profile in (7.8) corresponds to the wind stress that drives the ocean.

The contour plot of the initial mean stream function is presented in Fig. 1. It shows that the circulation profile is more concentrated around the western boundary area, because of the choice $r=0.05$.

There is no heat flux at the ocean surface, i.e., $\rho_f$ is set to be 0 in (2.5). Moreover, the boundary condition on lateral boundary sections is given by (2.4).

The Rossby number is taken to be 0.005, the Reynolds numbers are chosen to be $Re_1=750$, $Re_2=375$, $Rt_1=5{,}000$, $Rt_2=2{,}500$.

It is given in Figs. 2 and 3 the contour plots of the density field computed by the fourth-order method on the resolution of $256\times256\times128$ at $t=3,4$, respectively. Note that only the horizontal plots at $z=-0.125,-0.0625$ are present.

The circulation structure of the thermocline profile is clearly seen. Moreover, its interaction with the wind stress given by (7.8) is shown in the horizontal cut plots. Due to the choice of the initial mean stream function and the wind stress, a connection between the main thermocline structure and the western boundary layer is more and more obvious as the ocean depth is closer to the ocean surface.

It can be also observed that the vertical structure of two-layer stratification with an interface transition area keeps stable for a long time. The composition of the density profile always keeps the pattern of two layers with $\rho_1:\rho_2$, connected by an interface.

The plots for the mean stream function at the same time sequence is given in Fig. 4 below. It shows that a single circulation structure is bifurcated into several centers as time goes on, because of the nonlinear effects, along with the wind stress force.

At the final time $t=4$, the plots for the horizontal velocity $(u,v)$ at $z=-0.125,-0.0625$ are given in Figs. 5 and 6, respectively.

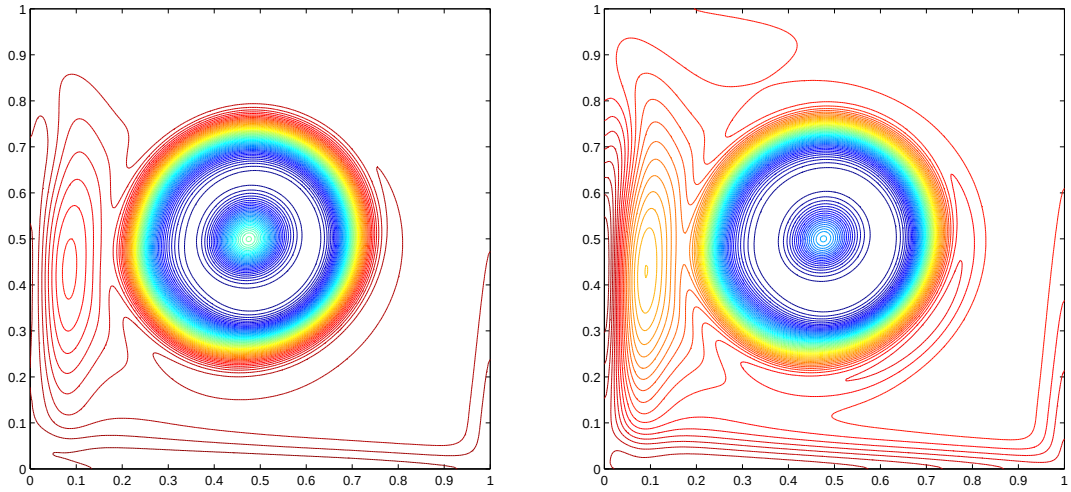

Figure 2: Density plots on $z=-0.125,-0.0625$, at the time $t=3$ with $Re_1=750$, $Re_2=375$, $Rt_1=5000$, $Rt_2=2500$. The computation is based on the fourth-order method with $256\times256\times128$ resolution.

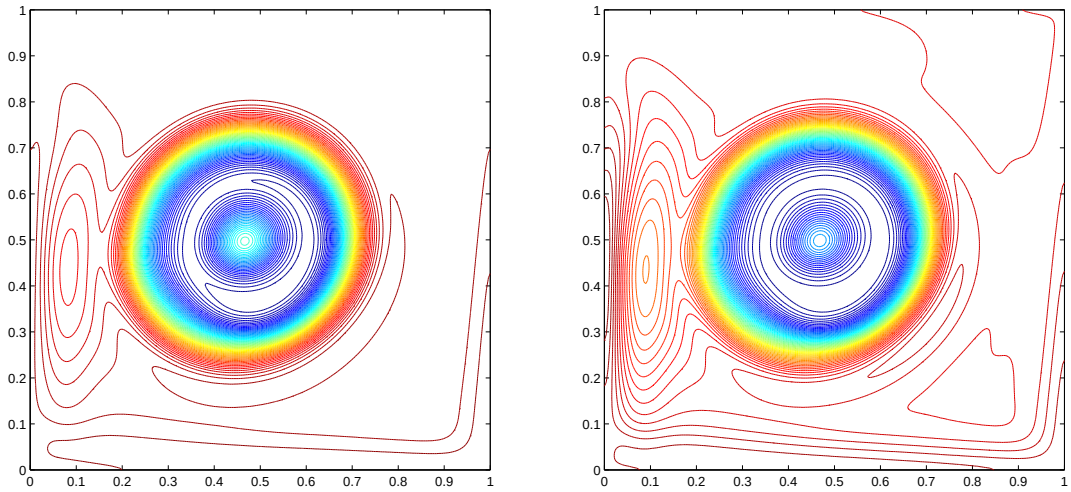

Figure 3: Density plots on $z=-0.125,-0.0625$, at $t=4$ with the same physical parameters in Fig. 2 and the same resolution.

From the numerical results in Figs. 5 and 6, we see that the horizontal velocity includes two primary parts. In the interior region, the structure is basically determined by an approximation to the geostrophic balance, i.e.,

$$fk\times\boldsymbol{v}+\nabla p=0, \tag{7.9}$$

which in turn indicates

$$fk\times\boldsymbol{v}_z-\nabla\rho=0, \qquad \text{i.e.} \quad (u_z,v_z)=\Big(\frac{\partial_y\rho}{f},-\frac{\partial_y\rho}{f}\Big). \tag{7.10}$$

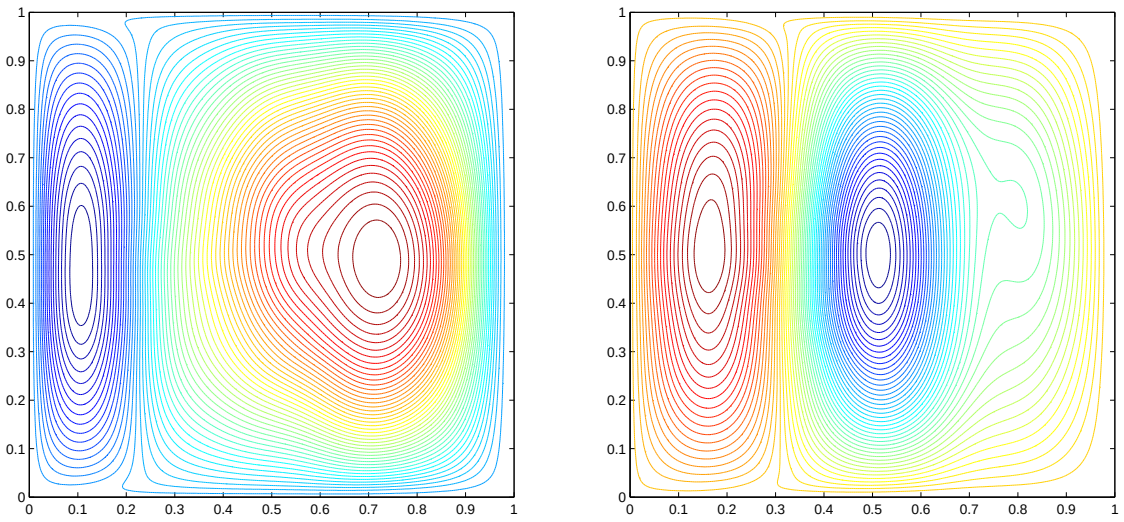

Figure 4: Plots for mean stream function at the sequence of time $t=3,4$.

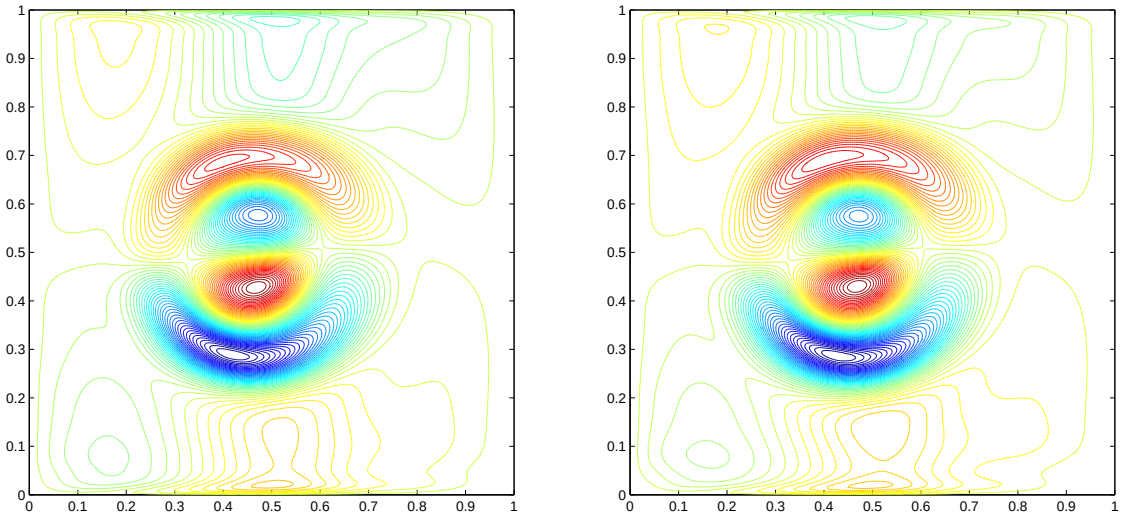

Figure 5: Contour plots for velocity $u$ on $z=-0.125,-0.0625$, at $t=4$.

Note that (7.9) and (7.10) are not exactly satisfied in the context of the PEs. Yet our numerical results show that the geostrophic balance is "approximately" satisfied if the depth is away from a thin boundary layer near the ocean surface, due to the choice of a small Rossby number $Ro=0.005$. Another important part in the composition of the horizontal velocity is influenced by the wind stress force, especially in the area near the ocean surface.

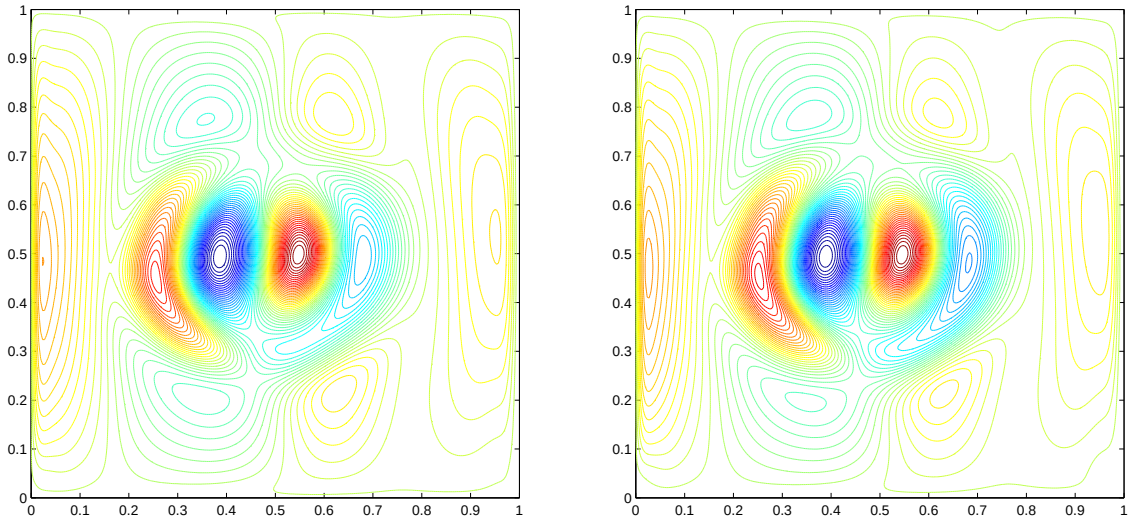

Figure 6: Contour plots for velocity $v$ on $z=-0.125,-0.0625$, at $t=4$.

## 8 Conclusion remarks

In this paper, a fourth-order finite difference method is developed for the three-dimensional primitive equations based on an equivalent formulation. An evolutionary equation for the mean vorticity field and the transport equations for the vertical derivative of the horizontal velocity are utilized to recover the total velocity vector. A fourth-order compact difference scheme is applied to approximate the mean vorticity equation to assure a numerical stability, along with a local vorticity boundary condition. Fourth-order long-stencil approximations are utilized to deal with transport type equations for $(\xi,\zeta)$ and the density, with a one-sided fourth-order boundary extrapolation for each variable. The robustness of the proposed fourth-order method is shown by a few numerical experiments, including an accuracy check and a large-scale oceanic circulation simulation.

A full fourth-order convergence analysis in the $L^\infty([0,t_1];L^2)$ norm for the velocity and density is expected in a future paper, which will be the first such result for three-dimensional primitive equations. In addition, to apply the current method to the simulation of large-scale oceanic flow with complicated coastlines and topographies, a finite element scheme based on the equivalent formulation has to be investigated in detail, using similar ideas as in [13]. This will lead to a better understanding of the circulation dynamics.

## Acknowledgments

The research of the first author was supported by the NSF grant DMS-0512176.

**References**

[1] P. Berloff and S. Meacham, The dynamics of an equivalent-barotropic model of the wind driven circulation, J. Mar. Res. **55** (1997), 523–563.
[2] D. Bresch, F. Guile'n-Gonza'lez, N. Masmoudi, and M. Rodri'guez-Bellido, Asymptotic derivation of a Navier condition for the primitive equations, Asymptot. Anal. **33** (2003), 237–259.
[3] D. Bresch, F. Guile'n-Gonza'lez, N. Masmoudi, and M. Rodri'guez-Bellido, On the uniqueness of weak solutions of the two-dimensional primitive equations, Differential Integral Equations **16** (2003), 77–94.
[4] W. Briley, A numerical study of laminar separation bubbles using the Navier-Stokes equations, J. Fluid Mech. **47** (1971), 713–736.
[5] K. Bryan, A numerical investigation of a nonlinear model of wind-driven ocean, J. Atmos. Sci. **20** (1963), 594–606.
[6] C. S. Cao and E. S. Titi, Global well-posedness of the three-dimensional viscous primitive equations of large scale ocean and atmosphere dynamics, Ann. Math. **166** (2007), 245–267.
[7] J.G. Charney, The dynamics of long waves in a baroclinic westerly current, J. Meteorol. **4** (1947), 135–163.
[8] J.G. Charney, Integration of the primitive and balance equations, Proc. Int. Symp. Numerical Weather Prediction (1962), Tokyo.
[9] J.G. Charney, R. Fj$\phi$rtaft, and J. Von Neumann, Numerical integration of the barotropic vorticity equation, Tellus **2** (1950), 237–254.
[10] B. Cushman-Roisin, Introduction to geophysical fluid dynamics, Prentice Hall, New-Jersy, 1996.
[11] J. K. Dukowicz and R. D. Smith, A reformulation and implementation of Bryan-Cox-Semtner ocean model on the connection machine, J. of Atmos. Oceanic Tech **10** (1993), 195–208.
[12] W. E and J.-G. Liu, Essentially compact schemes for unsteady viscous incompressible flows, J. Comput. Phys. **124** (1996), 368–382.
[13] W. E and J.-G. Liu, Simple finite element method in vorticity formulation for incompressible flow, Math. Comp. **70** (2001), 579–593.
[14] F. Guile'n-Gonza'lez, N. Masmoudi, and M. Rodri'guez-Bellido, Anisotropic estimates and strong solutions of the primitive equations, Differential Integral Equations **14** (2001), 1381–1408.
[15] W. R. Holland, The role of mesoscale eddies in the general circulation of the ocean, J. Phys. Oceanogr. **8** (1978), 363–392.
[16] C. Hu, R. Temam, and M. Ziane, Regularity results for GFD-Stokes problem and some related linear elliptic PDEs in primitive equations, Chinese Ann. of Math (CAM), Ser. B **23** (2002), 277–297.
[17] C. Hu, R. Temam, and M. Ziane, The primitive equations on the large scale ocean under the small depth hypothesis, Discrete Contin. Dyn. Syst.-Ser. A **9** (2003), 97–131.
[18] J. L. Lions, R. Temam, and S. Wang, New formulations of the primitive equations of the atmosphere and applications, Nonlinearity **5** (1992), 237–288.
[19] J. L. Lions, R. Temam, and S. Wang, On the equations of large-scale ocean, Nonlinearity **5** (1992), 1007–1053.
[20] J. L. Lions, R. Temam, and S. Wang, Models of the coupled atmosphere and ocean (CAO I), Computational Mechanics Advance **1** (1993), 3–54.
[21] J. L. Lions, R. Temam, and S. Wang, Numerical analysis of the coupled atmosphere and

ocean models (CAOII), Computational Mechanics Advance **1** (1993), 55–120.
[22] J. L. Lions, R. Temam, and S. Wang, Mathematical problems of the coupled models of atmosphere and ocean (CAOIII), Math. Pures et Appl. **73** (1995), 105–163.
[23] J. Pedlosky, Ocean circulation theory, Springer-Verlag, New York, 1983.
[24] J. Pedlosky, Geophysical fluid dynamics, second ed., Springer-Verlag, New York, 1987.
[25] L. F. Richardson, Weather prediction by numerical process, Cambridge University Press, New York, 1965.
[26] R. Samelson, R. Temam, C. Wang, and S. Wang, Surface pressure poisson equation formulation of the primitive equations: Numerical schemes, SIAM J. Numer. Anal. **41** (2003), 1163–1194.
[27] J. Shen and S. Wang, A fast and accurate numerical scheme for the primitive equations of the atmosphere, SIAM J. Numer. Anal. **36** (1999), 719–737.
[28] E. Simonnet, M. Ghil, K. Ide, R. Temam, and S. Wang, Low-frequency variability in shallow-water models of the wind-driven ocean circulation (I): Steady-state solution, J. Phys. Oceanogr. **33** (2003), 712–728.
[29] E. Simonnet, M. Ghil, K. Ide, R. Temam, and S. Wang, Low-frequency variability in shallow-water models of the wind-driven ocean circulation (II): Time-dependent solutions, J. Phys. Oceanogr. **33** (2003), 729–752.
[30] R. D. Smith, J. K. Dukowicz, and R. C. Malone, Parallel ocean general circulation modeling, Physica D **60** (1992), 38–61.
[31] S. Speich and M. Ghil, Interannual variability of the mid-latitude oceans: a new source of climate variability?, Sistema Terra **3**(3) (1994), 33–35.
[32] J. Strikwerda, Finite difference schemes and partial differential equations, SIAM, Philadelphia, 2004.
[33] C. Wang, The primitive equations formulated in mean vorticity, Discrete Contin. Dyn. Syst.Proceeding of "International Conference on Dynamical Systems and Differential Equations" **B4** (2002), 880–887.
[34] C. Wang and J.-G. Liu, Analysis of finite difference schemes for unsteady Navier-Stokes equations in vorticity formulation, Numer. Math. **91** (2002), 543–576.